의학박사 학위논문

Extracellular vesicles induce aggressive phenotype of luminal breast cancer cells by PKM2 phosphorylation

세포외 소포체에 의해 유도된 PKM2 인산화를 통한 관내강형 유방암 세포의 공격적 형질 획득

2020 년 8 월

서울대학교 융합과학기술대학원

분자의학 및 바이오제약학과

강 서 영

Extracellular vesicles induce aggressive phenotype of luminal breast cancer cells by PKM2 phosphorylation

지도교수 이 동 수

이 논문을 의학박사 학위논문으로 제출함

2020 년 5 월

서울대학교 융합과학기술대학원

분자의학 및 바이오제약학과

강서영

강서영의 박사학위논문을 인준함

2020 년 7 월

위 원 장	이 유 진	(인)
부 위 원 장	이 동 수	(인)
위 원	신 영 기	(인)
위 원	최 홍 윤	(인)
위 원	황 도 원	(인)

Abstract

Extracellular vesicles induce aggressive phenotype of luminal breast cancer cells by PKM2 phosphorylation

Seo Young Kang

Department of Molecular Medicine and Biopharmaceutical Sciences,

Graduate School of Convergence Science and Technology,

Seoul National University

Introduction: The aerobic glycolysis is a hallmark of cancer glucose metabolism. Several studies have suggested that cancer-derived extracellular vesicles (EVs) can modulate glucose metabolism in adjacent cells and promote disease progression. Here we suggest that EVs originated from breast cancer cell with high glycolytic activity can modulate glucose metabolism in the recipient breast cancer cells with relatively low glycolytic activity, and further induce cell proliferation.

Method: To demonstrate that tumor-derived EVs contribute to glucose metabolism in cancer cells, two types of breast cancer cell lines with different levels of glycolytic activity were selected. One is MDA-MB-231, a claudin Low-type breast cancer cell well known as a very aggressive breast cancer subtype. The other is MCF7, luminal type breast cancer cell, which has a relatively good prognosis. These cell lines,

MDA-MB-231 and MCF7, were co-cultured using indirect co-culture system such as transwell system or microfluidic system to confirm the changes in the glucose metabolism in the recipient cells, MCF7. Glucose analogue, ^{18}F-fluorodeoxyglucose (^{18}F-FDG) was used to evaluate basal glucose metabolic status of these cells. To determine the role of EVs, EVs isolated from MDA-MB-231 cells were put into MCF7 cells and cultured. Confocal fluorescence microscopy was used for evaluating the EVs signal in co-cultured MCF7 with MDA-MB-231-tdTomato. Immunoblotting was carried out with antibodies against crucial proteins - glucose transporter 1 (GLUT1) and pyruvate kinase M2 isoform (PKM2) - in glycolysis pathway. Phosphorylation at ^{105}Y of PKM2 was also evaluated to check inhibition of PKM2 activity in the co-cultured MCF7. Proteomics analysis was conducted to confirm the overall change in protein expression of co-cultured MCF7 and to identify proteins within EV derived from MDA-MB-231.

Results: Basal FDG uptake ratio of MDA-MB-231 and MCF7 cells at 60 min showed very big difference. FDG uptake ratio of MCF7 cells was markedly increased after indirect co-culture with MDA-MB-231 cells using transwell system. After 24 hrs culture with isolated EVs from MDA-MB-231 in the MCF7 cells, FDG uptake ratio was increased. CCK-8 assay showed increased cellular proliferation when isolated EVs were treated in the MCF7 cells. Fluorescence imaging of MCF7 after co-culture with MDA-MB-231-tdTomato cells showed multiple tdTomato signals inside the cell, which proved that EVs originated from MDA-MB-231-tdTomato were transferred to MCF7 cell. In addition, serine 37 phosphorylation of PKM2 necessary for tumorigenesis was markedly increased in co-cultured MCF7

cells and it mainly located in the nucleus. Tyrosine phosphorylation of PKM2 suggesting activated aerobic glycolysis was also increased in the co-cultured MCF7 cells. Proteomic profiling of the co-cultured MCF7 cells showed that proteins associated with cell differentiation decreased while gene expression and translation increased. In addition, proteomic analysis of EVs revealed that there were important proteins in the EV such as EGFR, ERBB2 and MAPK for phosphorylating PKM2.

Conclusions: EVs originated from MDA-MB-231 cells upregulated aerobic glycolytic activity by phosphorylating PKM2, which eventually induced cell proliferation in MCF7 cells. In co-cultured MCF7 cells, protein expression associated with cell proliferation were increased, while those related to cell differentiation was decreased. This phenomenon suggests the potential for aggressive cancer cells to affect other cancer cells through EV mediators.

Keywords: breast cancer cell, extracellular vesicles, aerobic glycolysis, PKM2 phosphorylation

Student number: 2014-30803

Contents

List of tables

List of figures

List of Abbreviations

Full name	Abbreviations
Triple negative breast cancer	TNBC
Extracellular vesicle	EV
Tumor microenvironment	TME
^{18}F-Fluorodeoxyglucose	FDG
positron emission tomography	PET
Pyruvate kinase	PK
Pyruvate kinase M2	PKM2
Glucose transporter 1	GLUT1
Phosphoenolpyruvate	PEP
Signal transducer and activator of transcription 5	STAT5
Lactate dehydrogenase A	LDHA
Glucose-6-phosphate isomerase	GPI
Epidermal growth factor receptor type	EGFR
Platelet-derived growth factor	PDGF
Extracellular matrix protein 1	ECM1
Extracellular-signal-regulated kinase	ERK
Dulbecco's modified Eagle's medium	DMEM

Palmitoylated-tdTomato	tdTomato
Polyethylene terephthalate	PET
Poly-dimethylsiloxane	PDMS
Extracellular matrix	ECM
Nanoparticle tracking analysis	NTA
Gene ontology	GO
Ingenuity Pathway analysis	IPA
Kyoto Encyclopedia of Genes and Genomes	KEGG
Data-dependent acquisition	DDA
False discovery rate	FDR
Liquid chromatography	LC
Mass spectroscopy	MS
Tandem Mass Tag	TMT
Conditioned media	CM

Introduction

Cell-to-cell communication in cancer

Cell-to-cell communication has well known to play a critical role during tumor progression and metastasis, allowing cancer cell to reprogram the surrounding tumor microenvironment (TME) (1, 2). The active crosstalk between cancer cells and tumor stroma consisting of immune and stroma cells, fosters various necessary processes for tumor progression and dissemination, including angiogenesis, cellular proliferation, immune-escape, formation of a pre-metastatic niche, invasion and multi-drug resistance (3, 4). Cell communication can be made through direct cell-to-cell interactions or the paracrine effect by soluble factors, such as cytokines, growth factors and chemokines (5). The most noteworthy way of communication between cancer cells and TME is the use of extracellular vesicle (EV) (6-8).

As a mechanism to communicate with the tumor microenvironment, tumor cells actively release large quantity of extracellular vesicles (EVs) that are a heterogeneous group of cell-derived membranous structures comprising exosomes and microvesicles (MVs) (9, 10). Exosomes are endosome-originated 50-150 nm small vesicles. MVs generated by the outward budding and fission of the plasma membrane have various size ranging from 50 nm to 1,000 nm in diameter (11, 12). These cancer cell-derived EVs, which are abundant in the body fluids of cancer patients, play a critical role in promoting tumor growth and progression through intercellular signaling (13, 14). Recently, several articles have been reported on the diagnosis and treatment of various diseases, and in particular on the role of EVs as

therapeutic targets (15-18).

There is a study reporting on the potential of cancer-derived EVs modifying glucose utilization of recipient cells (2). The result suggests that miR-122 which is transferred to the normal cells through the EV inhibits the pyruvate kinase M2 (PKM2) of the recipient cells and lowers the glucose transporter 1 (GLUT1) to limit the glucose utilization of the recipient cells. It was also suggested in several studies that cancer cell-derived exosomes foster the tumor-like phenotype transform of other cells by activating glycolysis (19-21).

Aerobic glycolysis

One thing to consider when we discuss activated glycolysis in cancer is the aerobic glycolysis, a characteristic glucose metabolism process of cancer. Aerobic glycolysis is a phenomenon observed by Otto Warburg that despite the availability of oxygen, most cancer cells produce energy predominantly by a high rate of glycolysis followed by lactic acid fermentation in the cytosol rather than by a comparatively low rate of glycolysis followed by pyruvate oxidation in the mitochondria (22-24). And the most important key molecule controlling aerobic glycolysis is pyruvate kinase (PK), which is precisely M2 isoform of pyruvate kinase (PKM2) (25-27).

Pyruvate kinase is the final rate-limiting protein of glycolysis and catalyzes the conversion of phosphoenolpyruvate (PEP) to pyruvate (28). There are multiple

pyruvate kinase isoforms including PKM1, PKM2, PKL, and PKR expressed in different types of mammalian cells and tissues. The PKM2, resulting from a specific spliced mRNA form, mainly acts on cancer cells and is a key regulator of aerobic glycolysis known as the Warburg effect. Increased expression and phosphorylation of PKM2 is a characteristic glycolytic phenotype of cancer cells, which promotes rapid energy production and flow of glycolytic intermediates into collateral pathways to synthesize nucleic acids, amino acids, and lipids (28-30). Gambhir group, who recognized the value of PKM2 in cancer, developed positron emission tomography (PET) tracers, ^{11}C- or ^{18}F-labeled PKM2 specific radiotracer (DASA-23), for visualizing PKM2 *in vivo* (31-34). In addition, several studies have focused on PKM2 as a strategy to explore new anticancer drugs, and studies have shown that they may increase anticancer effect or reduce anticancer drug resistance (35-37).

Although there are overwhelmingly many studies dealing with the interaction between cancer and stromal cells, studies have also been conducted to take into account the reciprocal interaction between cancer cells, albeit in a minority. Since there are various reports that breast cancer can consist of several subtypes within the tumor, the interaction between cancer cells in the tumor is well worth studying (38-40). Therefore, we investigate the role of EV modifying glucose metabolism in recipient cancer cells and major proteins inducing increased aerobic glycolysis, including PKM2, to figure out the reciprocal interactions between cancer cells.

Purpose

The purpose of this study was to evaluate the change of glucose uptake and activation of aerobic glycolysis in the recipient cancer cells after co-culture with more aggressive cancer cells. We used triple-negative breast cancer, MDA-MB-231 and luminal type breast cancer, MCF7 cells for analysis of reciprocal interaction between cancer cells.

Materials and Method

Cell culture and analysis

Cell lines and cell culture

HepG2 (human hepatocellular carcinoma), Hep3B (human hepatocellular carcinoma), SK-OV-3 (human ovarian cancer cell), HT-1080 (human fibrosarcoma cell), HFF (human fibroblast), MDA-MB-231(human triple negative breast cancer cell) and MCF7 cells (human luminal type breast cancer cell) were purchased from Korean Cell Line Bank. The cells were cultured in Dulbecco's modified Eagle's medium (DMEM) containing with 10% fetal bovine serum (FBS), 10 U/ml penicillin, and 10 μg/ml streptomycin under humidified 5% CO_2 atmosphere and at 37 ℃.

MDA-MB-231 were transfected with a lentiviral vector encoding the red fluorescent protein palmitoylated-tdTomato (tdTomato) using lipofectamine transfection reagent (Life Technologies). Supernatant recovered after 48h from 293T transfected cells was filtered by a 0.45 μm pore membrane and added to MDA-MB-231 plated cells supplemented with 4 μg/mL polybrene (Sigma-Aldrich). After viral infection, palm-td-Tomato positive cells were selected using FACS for stable integration of the transfects.

Transwell cell culture

To induce indirect co-culture of two cell lines, transwell inserts with a PET membrane of 0.4-μm pore size (BD Bioscience) were used. MDA-MB-231 cells (0.8

$\times 10^5$ cells per well) were plated on the lower wells and MCF7 or HFF (1×10^4 cells) were seeded into the top chamber (24-well insert; BD Bioscience) and then co-cultured for 24 hrs. All experiments were performed in triplicate.

Glucose uptake analysis

Glucose analogue, ^{18}F-fluorodeoxyglucose (FDG) was used to evaluate basal glucose metabolic status of these cells. After preculture for 4 hrs at glucose free media (glucose free DMEM, Gibco), cells were washed 3 times with PBS and cultured at 0.2 μCi of ^{18}F-FDG with PBS for 1 hr at 37℃ in 5% CO2. Cells were then harvested using 0.5% SDS solution and FDG uptake was measured using gamma counter (Packard Cobra-II Auto gamma counter). All experiments were performed in triplicate.

Heparin treatment

MCF7 cells pre-cultured with heparin at concentrations of 0.1, 0.2, and 1 ng/ml, respectively, were seeded on microfluidic chips with MDA-MB-231 cells. During the 24 hrs co-culture, the heparin concentration in the medium was maintained.

Lactate assay

The levels of lactate production were examined with a Lactate Assay Kit (DG-LAC200, DoGenBio, Korea). MDA-MB-231 cells (5×10^4 cells per well) were plated in 24-well culture plate and the top chamber (24-well insert; BD Bioscience) were seeded with MCF7 (2×10^4 cells) and then co-cultured for 24 hrs. After incubation for 24 hrs, lactate assays were performed with culture media collected from each sample according to the manufacturer's protocol and the optical density was measured at 450 nm using a microplate reader (GloMax®-Multi E7031, Promega)

Microfluidic system

Microfluidic Device Fabrication

A microfluidic device was established by the method mentioned in the previous report (41). It was manufactured by bonding Microchannel-patterned PDMS (poly-dimethylsiloxane; Sylgard 184; Dow Corning) to a glass coverslip. The conventional soft-lithography process was used to replicate the microchannel-patterned PDMS with SU-8 photoresist pattern master as a master mold (MicroChem). The PDMS elastomer, which was completely mixed with the curing agent at 10:1 weight ratio, was poured into the wafer and baked for 1 h 30 min in an oven at 80 ℃. After curing, the PDMS replicas were removed from the wafer and all reservoir patterns on the PDMS replica were punched using skin biopsy punches. The sterilized PDMS replicas and glass coverslip were glued through oxygen plasma (Femto Science) and placed in the oven at 80 ℃ for at least 24 hrs to restore hydrophobicity of the microchannel surfaces.

Co-culture of MDA-MB-231 and MCF7 cells in the microfluidic system

Type 1 collagen ECM (2 mg/ml; BD Biosciences) was injected into the hydrogel channel and gelled in a 37℃ incubator for 30 min. Cell seeding was then prepared by adding medium to the microfluidic channel and incubated at 37℃. MDA-MB-231 cells (donor cells, 200μL, 1×10^6 cells/mL) were seeded in one reservoir of the cell culture channel (left channel) and MCF7 cells (recipient cell, 200μL, 1×10^6 cells/mL) was seeded into the other reservoir of the cell culture channel (right channel). After cell attachment, in both reservoir of the culture channel, the medium was added and incubated at 37 ℃ in 5% CO_2 atmosphere for 24 hrs.

Preparation and characterization of Extracellular Vesicles (EV)

Extracellular vesicles from MDA-MB-231 were isolated using ultracentrifugation method. Filtered conditioned media was centrifuged in a Beckman Coulter Optima™ Ultracentrifuge at 150,000g at 4°C for 120 min with a Type 70 Ti rotor to pellet EVs. The supernatant was carefully removed, and crude EV-containing pellets were resuspended in ice-cold PBS and pooled. The amount of EV was estimated using the bicinchoninic acid assay (BCA; Thermo Scientific). Nanoparticle tracking analysis (NTA) system (NANOSIGHT NS500; Malvern) was used for measurement of EV size distribution and particle number. For optimal analysis, EVs were diluted with 1000-fold in particle-free PBS in the field of view.

A laser beam of the system was adjusted to focus a suspension of the particles of interest. All measurements were recorded for further analysis by NTA software.

Immunoassay

Immunoblotting

Cells were lysed in RIPA buffer, and centrifuged at 12,000 rpm for 30 min to remove cell debris. Protein concentration was measured using a BCA protein assay kit (Thermo Scientific). Equal amounts of protein per each sample were resolved by SDS-PAGE and transferred onto PVDF membranes (Millipore). The membrane was probed with rabbit monoclonal antibodies that recognize CD63 (1:1000; sc-5275; Santa Cruz biotechnology), CD81 (1:1000; sc-166029; Santa Cruz biotechnology), TSG101 (1:1000; ab83; Abcam), GLUT1 (1:1000; D3J3A; Cell Signaling), PKM2 (1:1000; D78A4; Cell Signaling), anti-phospho Y105 PKM2 (1:1000; ab156856; Abcam) overnight at 4 °C. Membranes were incubated with HRP-conjugated anti-rabbit secondary antibody for 2 h at room temperature, and proteins were visualized with a chemiluminescence detection system (Promega). Band intensities were quantified using AlphaView Software and results are expressed relative to the control condition. Three independent experiments were performed and the cropped version of the representative case of triplet is presented in the figures.

Immunocytochemistry

MCF7 cells co-cultured with MDA-MB-231 at transwell insert and microfluidic device were fixed with 4% paraformaldehyde (PFA) in PBS for 15 min at room temperature. The cells were then washed 3 times with PBS and treated with 0.5% Triton X-100 in PBS for 5 min at 4 ℃ to permeabilize cells. The samples were washed 3 times with PBS and non-specific binding sites were blocked with 5% BSA in PBS for 1 h at room temperature. Anti-rabbit GLUT1 (1:100; ab15309; Abcam), anti-rabbit PKM2 (1:100; D78A4; Cell Signaling), anti-rabbit phospho-PKM2 (1:100; PA5-78107; Thermo Fisher Scientific) antibodies were diluted in PBS and incubated with the samples at 4 ℃ overnight. In microfluidic system, diluted primary Abs were added into the microchannels and incubated at 4 ℃ overnight. The samples were then washed 3 times with PBS and incubated with Alexa Fluor 488-conjugated anti-rabbit secondary antibodies (1:10000; A32731; Invitrogen) for 1 h at room temperature to visualize the antibody reactions. Cell nuclei were stained using VECTASHIELD® mounting medium with DAPI (Vector Laboratories). Fluorescent images were acquired using a confocal laser scanning microscope (Leica TCS STED CW).

Proteome profiling of cell lysates and extracellular vesicles

Cell culture and preparation of EV

Two cell lines, MDA-MB-231 and MCF7, cultured in DMEM medium containing 10% FBS, 100 μg/mL streptomycin and 100 U/mL penicillin using transwell inserts for in-direct col-culture. MDA-MB-231 cells (0.8×10^5 cells per

well) were plated on the lower wells of 24-well plate and the top chamber were seeded with MCF7 (1×10^4 cells) and then co-cultured for 24 and 48 hrs. EV were isolated from MDA-MB-231 with same method as mentioned above.

Protein extraction

Proteins were extracted from the samples of both single-cultured and co-cultured MCF7 cells as well as EV originated from MDA-MB-231 cells in triplicate. The cell pellets were washed three times with cold PBS and lysed with 300 µl of lysis buffer (% SDS, 1 mM TCEP in 0.1 M TEAB pH 8.5). Protein concentration was measured using a BCA reducing agent compatible assay kit (Thermo Scientific, Rockford, IL, USA). Proteins were precipitated by adding ice-cold acetone overnight. Precipitated proteins were dissolved in 30 µl denaturation buffer (4% SDS and 100 mM DTT in 0.1M TEAB pH 8.5). After heating at 95℃ for 15 min, denatured proteins were loaded onto 30 kDa amicon filter (Merck Millipore, Darmstadt, Germany). The buffer was exchanged with UA solution (8 M UREA in 0.1 M TEAB pH 8.5) by centrifugation at 14,000 g three times. After removal of SDS, cysteine alkylation was achieved by adding an alkylation buffer (50 mM IAA, 8 M UREA in 0.1 M Tris-HCl pH 8.5) for 1 hour at room temperature in the dark. Additional buffer exchanges were performed with 40mM TEAB pH 8.5 three times. The proteins were digested with trypsin (enzyme-to-substrate ratio [w/w] of 1:100) at 37℃ overnight. The digested peptides were collected by centrifugation and the peptide concentrations were measured by tryptophan assay.

LC-MS/MS analysis and data processing for MCF7 cells

We distributed the 9 samples (3 groups of MCF7 cells with biological triplicate) to one TMT 10-plex set. Each 50 μg peptide sample was spiked with a uniform volume of ovalbumin. Subsequently, 40 mM TEAB buffer was added to each sample to equalize the volume. To eliminate errors caused by reagents, one set of TMT reagent was dissolved and spiked equally for the experiment. TMT reagent (0.8 mg) was dissolved in 110 μl of anhydrous ACN, of which 25 μl was added to the same channel in the experimental set. Then, 35 μl of ACN was added to achieve a final concentration of 30%. After incubation at room temperature for 1 hour, the reaction was quenched with hydroxylamine to a final concentration of 0.3% (v/v). The TMT-labeled samples were pooled at a ratio of 1:1 across all samples. The sample was lyophilized to almost dry and a desalting procedure was performed. The TMT-labeled peptide samples were desalted using solid phase extraction (SPE) column and high-pH peptide fractionation was performed by offline HPLC. Peptide samples were separated in a linear gradient and finally the sample was fractionated into 12 fractions. The fractions were lyophilized and stored at -80℃ until MS analysis. The fractionated peptide samples were analyzed by LC-MS/MS system, a combination of an Easy-nLC 1000 (Thermo Fisher Scientific, Waltham, MA) connected to a nano electrospray ion source (Thermo Fisher Scientific, Waltham, MA) on Q-Exactive plus mass spectrometer (Thermo Fisher Scientific, Waltham, MA).

MS raw files were processed using Proteome Discoverer 2.1 software based on the SEQUEST-HT search engine against the Human Uniprot database. Database searches were performed using a 10-ppm precursor ion tolerance and a 0.02Da

MS/MS ion tolerance. TMT tags on lysine residues and peptide N-termini and carbamidomethylation of cysteine residues were established as fixed modifications, while oxidation of methionine residues was set as a variable modification.

Statistical tests of the proteome were performed using Perseus software (42). After log2 transformation of the ion intensity, quantification was performed with a false discovery rate (FDR)-adjusted p-value < 0.05 with minimal fold-changes of ± 1.2. A comparative analysis between the single-cultured and co-cultured MCF7 cells identified total 57 differentially expressed proteins. There were 15 proteins identified in the first 24 hours, but eight more were found in the next 24 hours. Thirty-three more proteins were identified on a 48-hour incubation basis. Hierarchical clustering analysis revealed five clusters differentially expressed by co-culture duration among three groups. To functionally classify proteins of co-cultured MCF7 cells observed to be highly expressed relative to the single-cultured MCF7 cells in the proteomics data, we performed a gene ontology (GO) term analysis using Ingenuity Pathway Analysis (IPA, https://www.creative-proteomics.com/services/ipa-service.htm) (43) based on Uniprot database (http://www.uniprot.org/). Pathways were analyzed using the Kyoto Encyclopedia of Genes and Genomes (KEGG) databases. Protein-protein interactions (PPIs) for the network analysis were interrogated from STRING database (http://www.string-db.org) (44).

LC-MS/MS analysis and data processing for EVs from MDA-MB-231 cells

LC-MS/MS analyses were conducted with an Ultimate 3000 UHPLC system (Dionex, Sunnyvale, CA, USA) coupled to a Q-Exactive Plus mass spectrometer (Thermo Fisher Scientific, Waltham, MA). The column eluent was delivered to the Q-Exactive Plus via nanoelectrospray. In the data-dependent acquisition (DDA) method for label-free quantification, a survey scan (350 to 1650 m/z) was acquired with a resolution of 70,000 at m/z 200. A top-20 method was used to select the precursor ion with an isolation window of 1.2 m/z. The MS/MS spectrum was acquired at an HCD-normalized collision energy of 30 with a resolution of 17,500 at m/z 200. The maximum ion injection times for the full and MS/MS scans were 20 and 100 ms, respectively.

The raw LC-MS/MS data were analyzed using MaxQuant software (http://maxquant.org/, version 1.5.3.17) and searched against Human UniProt protein sequence database. Carbamido-methylation of cysteine was designated as a control variant, and N-acetylation of protein and oxidation of methionine were considered variable variants. Peptides with a minimum length of 6 amino acids and a maximum of 2 missing cuts were included. The acceptable false discovery rate (FDR) was set to 1% at the peptide, protein, and modification levels. For label-free quantification, an Intensity Based Absolute quantification (iBAQ) algorithm was used as part of the MaxQuant platform. The iBAQ values calculated by MaxQuant are the raw intensities divided by the number of theoretically observable peptides. Thus, the iBAQ values are provided in proportion to the molar amount of protein. Functional analysis of cargo proteins inside EVs was determined by GO enrichment of biological processes, molecular pathways and functions using the Functional

Enrichment analysis tool (FunRich) version 3.1.3 (Funrich Industrial Co. Ltd, Hong Kong) (45, 46). The inter-protein pathways were analyzed using KEGG and the PPIs of network model were visualized using Cytoscape (47).

Statistical analysis

All of the results were obtained from at least three independent experiments. Data are displayed as means ± standard deviation (SD). Comparison of results from experimental groups versus control groups were performed using performed using Prism (v8.0, GraphPad Software Inc.). A p-values of < 0.05.was considered statistically significant.

Results

Part I. MDA-MB-231 cells increased glycolytic activity of MCF7 cells through indirect co-culture

MDA-MB-231 cells increased glycolytic activity of MCF7 cells through indirect co-culture

Since human cancer cells have various glycolytic activity according to their aggressiveness, we compared glucose utilization status using glucose analogue, FDG, in several different cancer cell lines: MCF7, MDA-MB-231, HepG2, Hep3B, HT-1080, and SK-OV-3. As shown in Figure 1, these cell lines showed various FDG uptake. To rule out the potential effects of high glucose media, we compared the effect of glucose uptake by the culture media. With DMEM including high glucose, MDA-MB-231 cells resulted in more increased FDG uptake, whereas Hep3B and HepG2 cells showed more increased FDG uptake with MEM including relatively low glucose. MCF7 cells did not represent significant difference. Although there is a difference in the FDG uptake by the culture medium, there is no difference in the overall tendency of the cellular uptake (Figure 2).

We selected two hepatoma cell lines, HepG2 and Hep3B to evaluate the change of FDG uptake according to co-culture between two cell lines. Hep3B is well known as aggressive hepatocellular carcinoma with high glycolytic activity, whereas HepG2 has relatively low glycolytic activity (Figure 3a). After co-culture with more aggressive cancer cell, Hep3B in transwell system, HepG2 showed increased FDG

uptake compared to when cultured alone (Figure. 3b). We also compared the change of glycolytic activity in other cancer cell lines: luminal type breast cancer cell, MCF7 and triple negative breast cancer (TNBC) cell, MDA-MB-231. As we expected that TNBC cells are more aggressive and show increased glycolysis, The figure shows different glucose uptakes for various cancer cell types.

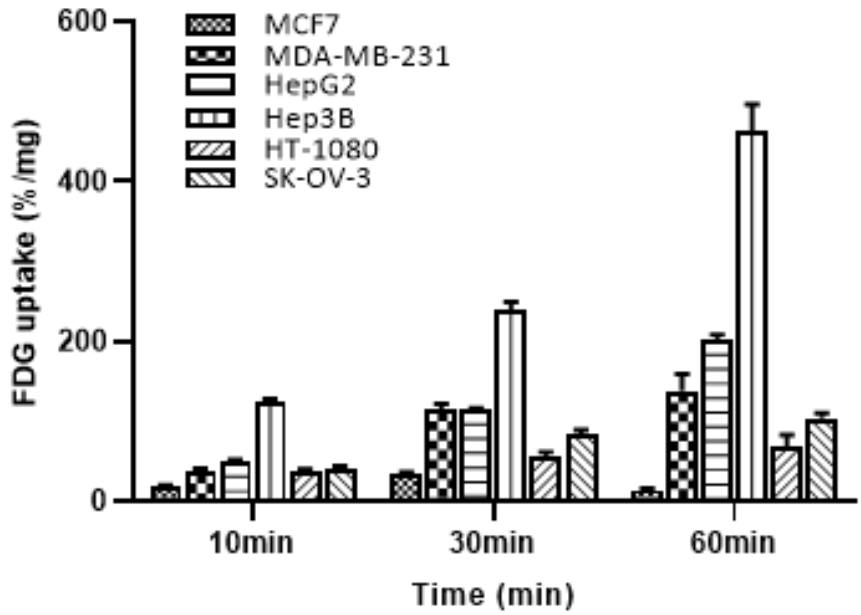

Figure 1. Baseline FDG uptake of various cancer cell lines.

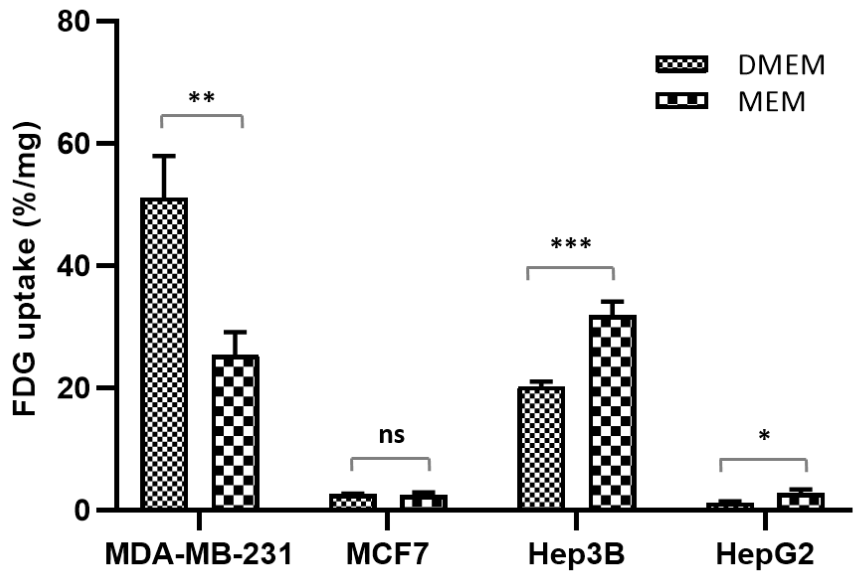

Figure 2. Evaluation of FDG uptake depending on glucose amount in the medium.

There is a difference in FDG uptake by the culture medium, but not the overall tendency of cell uptake.

*, $p<0.05$; **, $p<0.01$; ***, $p<0.001$;

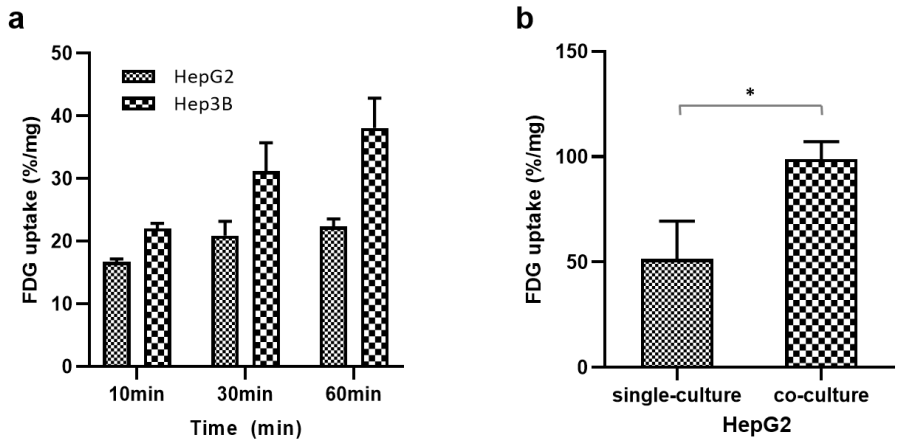

Figure 3. The change of glucose uptake in the HepG2 cell after co-culture with Hep3B cell.

Compared to baseline level of HepG2 cell, FDG uptake of HepG2 co-cultured with Hep3B was significantly increased.

*, $p<0.05$

MDA-MB-231 showed increased FDG uptake compared to MCF7 cells which have known as relatively less aggressive breast cancer cell (Figure 4a). We examined the change of metabolic phenotypes such as glucose uptake and lactate production that represents an activated aerobic glycolysis in MCF7 cell after co-culture with MDA-MB-231 using transwell system. Again, MCF7 cells co-cultured with MDA-MB-231 for 24 hrs showed dramatically increased FDG uptake compared to baseline level of MCF7 cell (Figure 4b). More high level of lactate production suggesting activated aerobic glycolysis was also observed in co-cultured MCF7 cells compared to baseline of MCF7 cell (Figure 5). On transwell experiment, transwell chambers of 0.4 μm pore size allowed passage of exosomes but not of larger vesicles (ranging 0.5 ~ 1 μm in diameter) or apoptotic bodies (> 1 μm in diameter). Therefore, we could deduce that EVs, especially exosomes secreted from MDA-MB-231 cell made alteration of glycolytic activity in the recipient MCF7 cell. To confirm our inference, we used heparin, which is known to interfere with EV uptake in recipient cells. The lowest heparin concentration tested, 0.1 μg/ml, achieved a 25 % reduction of FDG uptake in MCF7 cells co-cultured with MDA-MB-231 cells, and 50% reduced with 1ug/ml (Figure 6). In addition, manumycin-A (MA) which suppresses exosome biogenesis and secretion was treated in cells of co-culture to investigate the effect of inhibition of EV production (41, 48). MA of 2uM and 5uM induced decreased tendency of FDG uptake in MCF7 co-culture with MDA-MB-231 cells, though not statistically significant. MDA-MB-231 cells did not manifest any particular change relation to MA treatment (Figure 7).

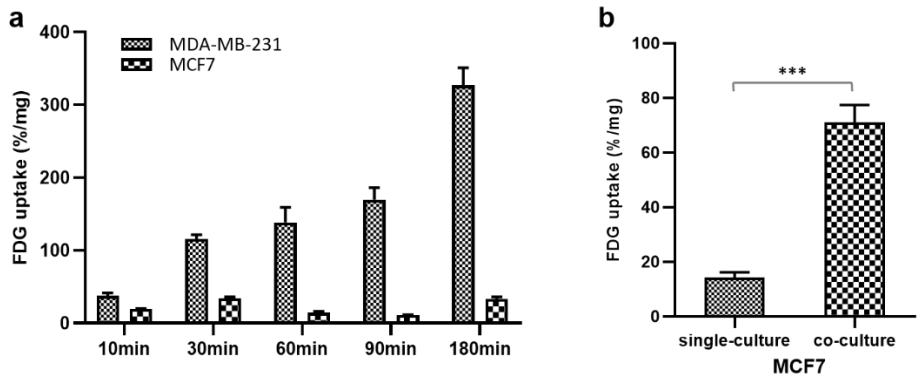

Figure 4. The change of glucose uptake in the MCF7 cell after co-culture with MDA-MB-231 cell.

baseline FDG uptake of two breast cancer cell lines; e, The change of FDG uptake in MCF7 cell after co-culture with MDA-MB-231; f, lactate assay in MCF7 cells after co-culture with MDA-MB-231; g, The change of FDG uptake increased by inhibiting EV uptake in MCF7 cells.

*, $p<0.05$; **, $p<0.01$; ***, $p<0.001$;

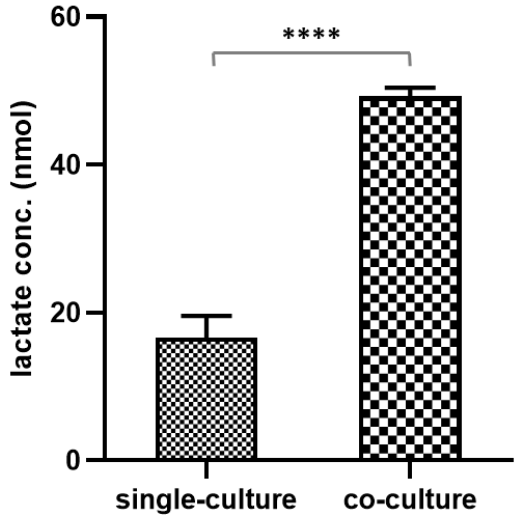

Figure 5. The change of lactate concentration in the MCF7 cell after co-culture with MDA-MB-231 cell.

Lactate concentration was significantly increased in the MCF7 cell co-cultured with MDA-MB-231 cell.

****, $p<0.0001$

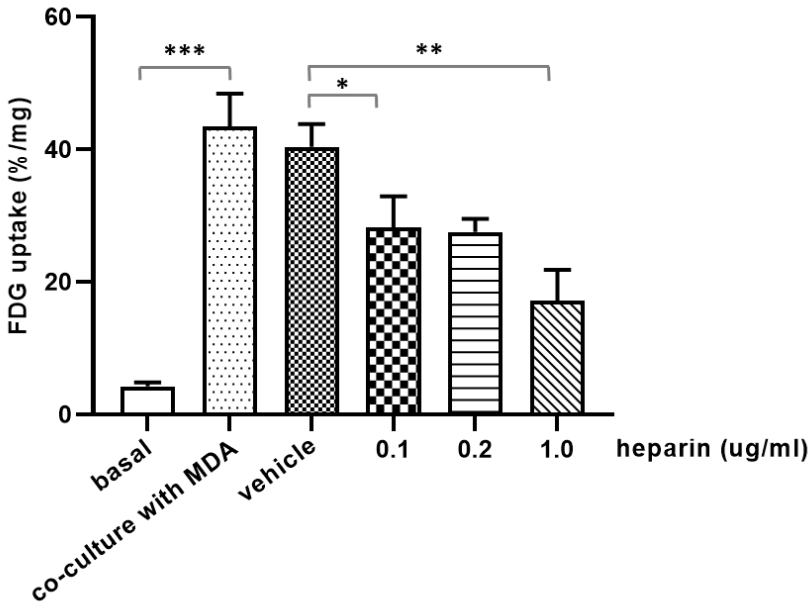

Figure 6. The change of FDG uptake by inhibiting EV uptake in MCF7 cells.

By treatment with heparin, the degree of increase in FDG uptake was reduced in MCF7 cells co-cultured with MDA-MB-231 cells. The FDG uptake was reduced by 25% from the heparin concentration of 0.1μg/ml and by 50% to 1ug/ml.

*, $p<0.05$; **, $p<0.01$; ***, $p<0.001$;

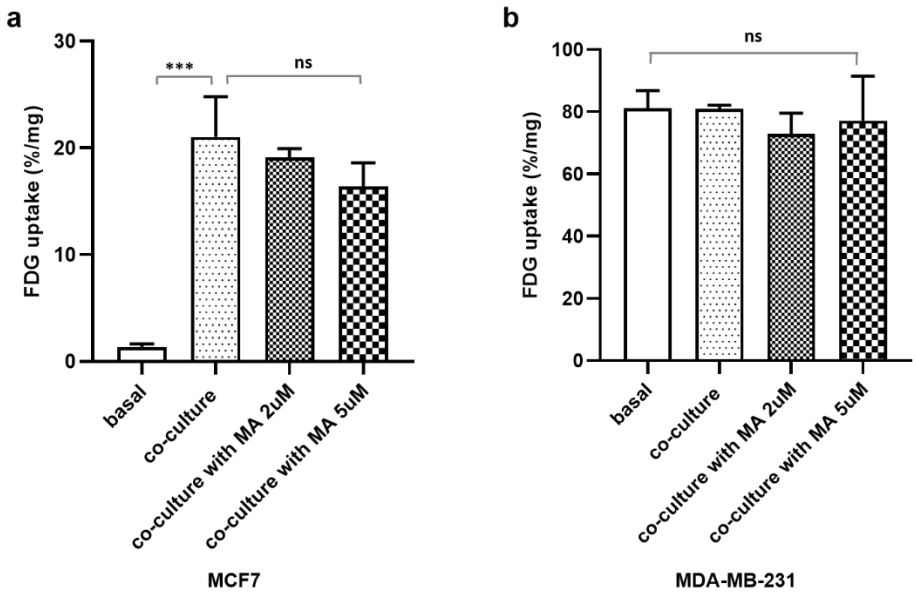

Figure 7. The change of FDG uptake in cell by inhibiting EV secretion in MDA_MB-231 cells.

Change of FDG uptake in MCF7 cells (a) co-culture with MDA-MB-231 cells (b) accodring to inhibition of EV secretion using manumycin-A.

ns, not significant; ***, $p<0.001$;

We also evaluated the effect of HepG2 and MCF7 cells on Hep3B and MDA-MB-231 cells. After co-culture with HepG2 and MCF7 cells in transwell system, respectively, FDG uptake of Hep3B and MDA-MB-231 cells did not significantly change compared to when cultured alone (Figure 8). While it is difficult to identify all the effects of relatively less aggressive cancer cells on more aggressive cancer cells, it has been confirmed that the glycolytic activity has not change much.

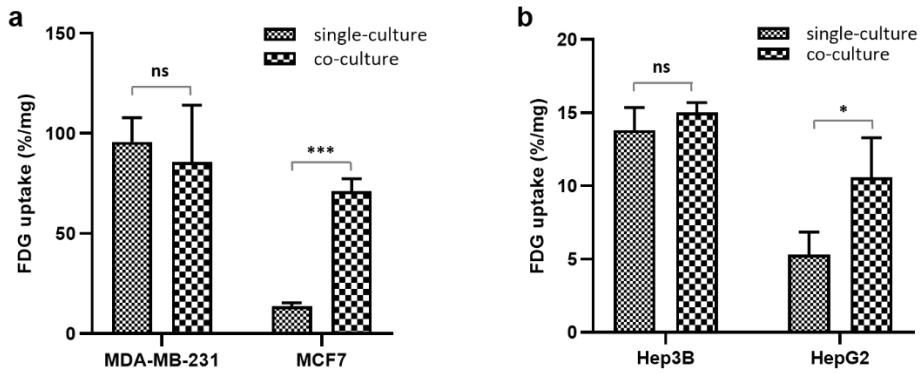

Figure 8. Changes in FDG uptake by co-culture between two cell lines, MDA-MB-231 and MCF7 (a), also Hep3B and HepG2 (b).

ns, not significant; *, $p<0.05$; ***, $p<0.001$;

EVs originated from MDA-MB-231 induces aerobic glycolysis in MCF7 cells

We postulated that EVs transported from MDA-MB-231 to the recipient MCF7 induced the change of glucose metabolism in the MCF7. First, we visualized MDA-MB-231-tdTomato cell-derived EVs inside MCF7 cells through co-culture using microfluidic chips mimicking interstitial fluid inside tumor distinct from macroscale transwell. Recipient MCF7 and donor MDA-MB-231-tdTomato cells were sequentially seeded 2-dimensionally in each channel and cultured for 24 hrs. Figure 9 showed that multiple red dot signals suggesting MDA-MB-231-tdTomato cell-derived EVs inside MCF7 cell and also in the channel between two cells of microfluidic chip (Figure 10). Next, we isolated EVs from MDA-MB-231 cells using ultracentrifugation and nanoparticle-tracking analysis (NTA) of the isolated EVs showed a uniform size with the diameter of 80-150 nm (Figure 11). To verify the isolated EVs, expression of exosome-marker proteins, including CD63, CD61 and *TSG101*, was confirmed using western blot (Figure 12). FDG uptake of MCF7 treated with MDA-MB-231-derived EVs was significantly increased at concentration of 100 ug/ml (Figure 13a) and CCK-8 assay showed increased cellular proliferation with EVs (Figure 13b). To confirm whether MDA-MB-231-derived EVs regulates glucose metabolic phenotype in MCF7, we examined the change of FDG uptake in various culture condition of MCF7 using EVs secreted from and EV-depleted conditioned media (EdCM) from MDA-MB-231 and HFF, respectively. MDA-MB-231-derived EV increased FDG uptake in MCF7 cells, although not as much as co-cultured. However, HFF-derived EVs did not induce a significant increase of FDG uptake. In addition, FDG uptake of MCF7 cultured in EdCM from

two cell lines was slightly increased compared to baseline uptake of MCF7. Since the EdCM effects derived from the two cells did not show much difference, it seems likely to be non-specific effect caused by the growth factors secreted by the cells. (Figure 14).

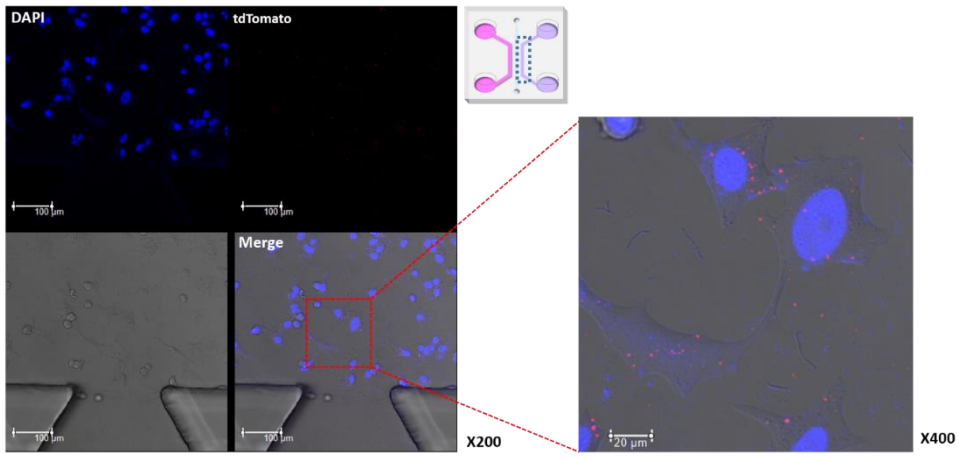

Figure 9. Fluorescence images shows tdTomato-EVs signals inside MCF7 cell co-cultured with MDA-MB-231-tdTomato cell.

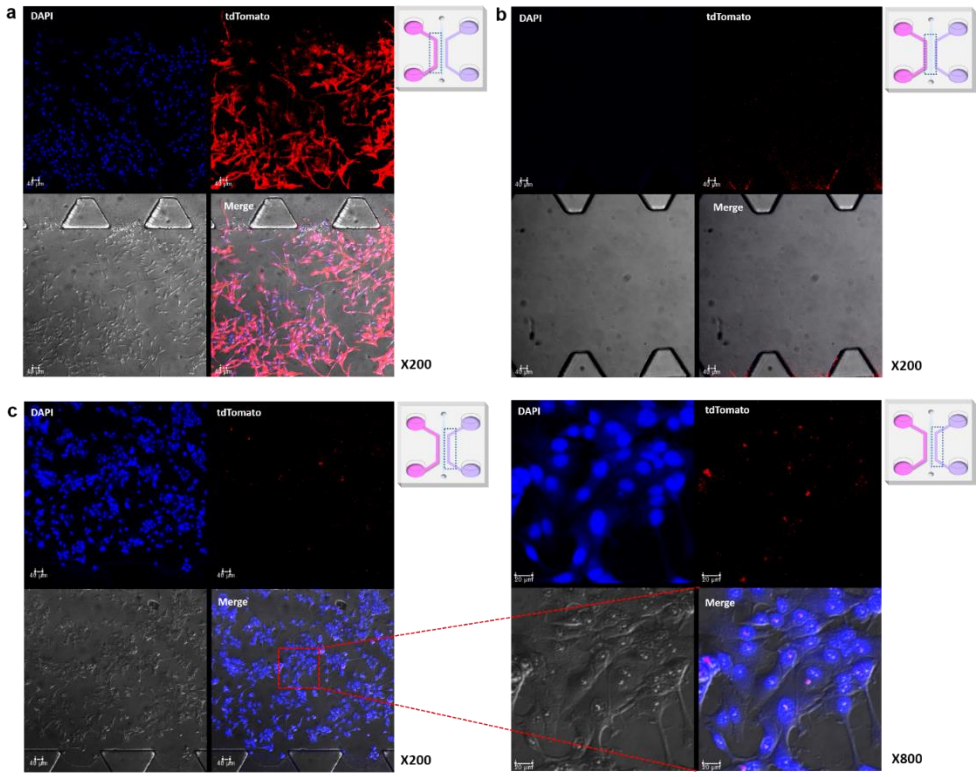

Figure 10. Fluorescence images of MDA-MB-231-tdTomato cells and tdTomato-EVs in the donor (a), middle (b) and recipient channels (c) of microfluidic chip.

There are MCF7 cells with tdTomato-EVs inside them in the recipient channel (c).

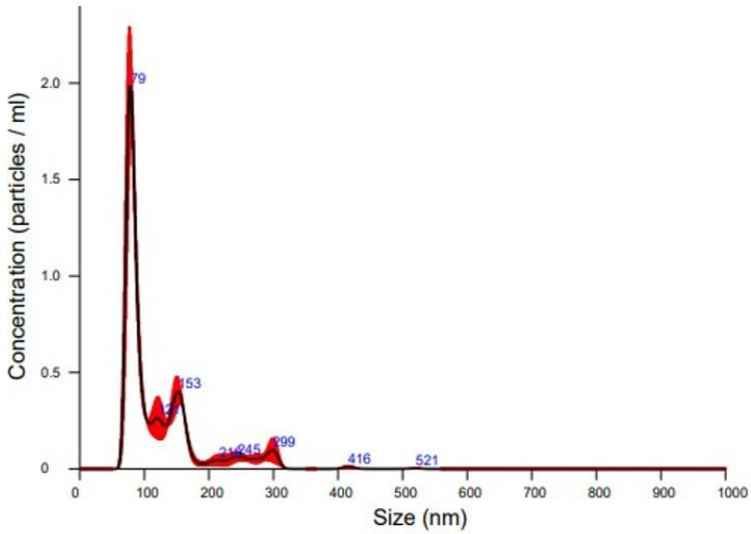

Figure 11. Characterization of isolated EVs from MDA-MB-231 cell.

Nanoparticle tracking analysis of isolated EVs was performed using Nano-Cyte®.

The main peak was 79nm, suggesting that most EVs are made up of exosomes.

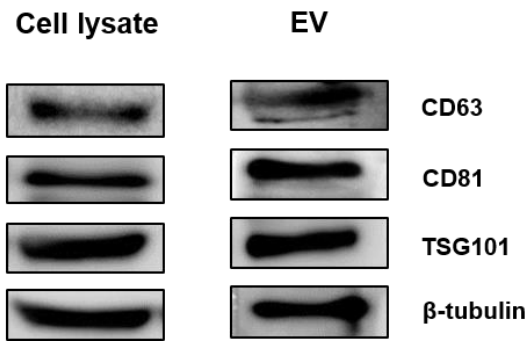

Figure 12. EV marker expression in isolated EVs from MDA-MB-231 cell.

The commonly used EV markers CD63, CD81 and TSG101 were detected in the isolated EV fraction as well as cell lysate.

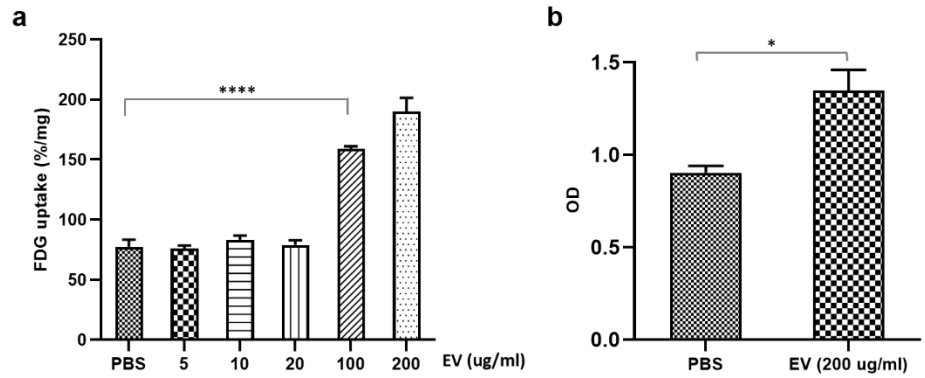

Figure 13. FDG uptake of MCF7 cell treated with MDA-MB-231-derived EVs.

FDG uptake of MCF7 cell was significantly increased at concentration of 100 ug/ml MDA-MB-231-derived EVs (a). CCK-8 assay showed increased cellular proliferation of MCF7 cell with EVs (b).

*, $p<0.05$; ***, $p<0.001$;

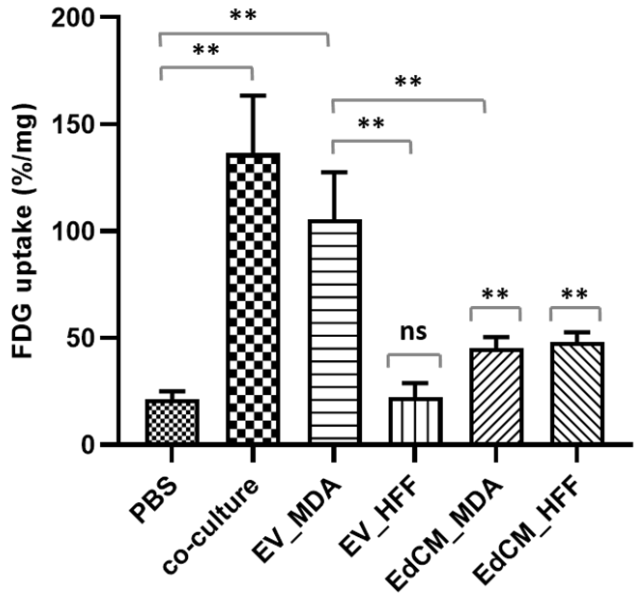

Figure 14. The effect of MDA-MB-231-mediated EVs compared to control groups such as EV-deprived conditioned medium and HFF-derived EVs.

Unlike MDA-MB-231 derived EVs that increased FDG absorption in MCF7 cells, HFF derived EVs did not significantly induce FDG absorption. EdCM in two cell lines has slightly increased FDG absorption, but it is likely to be an unspecified effect caused by the growth factor secreted by the cell, given that the EdCM effect derived from the two cells did not show much difference.

ns, not significant; **, $p<0.05$; MDA, MDA-MB-231; HFF, human fibroblast cell line; EdCM, EV-depleted conditioned media

When HFF was co-cultured with MDA-MB-231 cells, FDG uptake of HFF as well as MDA-MB-231 cells did not changed significantly. MDA-MB-231-derived EVs induced increased FDG uptake at concentration of 200 ug/ml in HFF cells, but no proliferation of HFF cells. Increased FDG uptake induced by high concentrations of EVs may be due to mass effects, and as in MCF7 cells, close interactions between cells do not seem to occur smoothly (Figure 15).

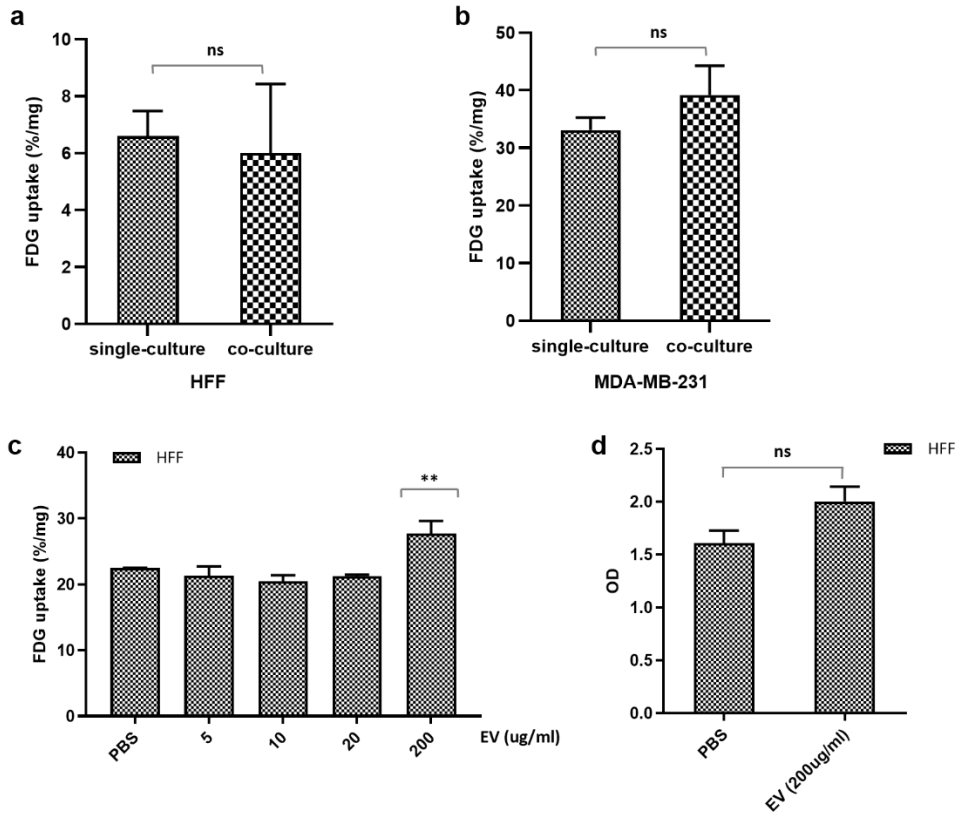

Figure 15. Change of FDG uptake in the HFF cells.

Change of FDG uptake in HFF cells (a) co-cultured with MDA-MB-231 cells (b); MDA-MB-231-derived EVs have significant effect of FDG uptake in HFF cells (c); MDA-MB-231-derived EVs did not activate proliferation in HFF cells (d) unlike in MCF7 cells.

ns, not significant; **, $p<0.05$;

Part II. PKM2 phosphorylation plays a critical role in the modulation of glucose metabolism

Serine phosphorylation of PKM2 was activated in the co-cultured MCF7

To investigate key proteins that induced increased glucose uptake, we selected two representative proteins in glycolysis pathway: glucose transporter 1 (GLUT1) and pyruvate kinase muscle isozyme M2 (PKM2). GLUT1 is primarily responsible for the uptake of glucose into cancer cells. PKM2 is a rate-limiting glycolytic enzyme that catalyzes the final step in glycolysis, which is key in tumor metabolism and growth. Tyrosine phosphorylation of PKM2 results in an interesting, paradoxical effect, where phosphorylation decreases PKM2 activity, and this decrease in activity promotes increased glycolytic flux and lactate production in cancer cells (49). Immunofluorescence analysis visualized GLUT1 and PKM2 in MCF7 cells as well as co-cultured with MDA-MB-231-tdTomato cells. Depending on their function, GLUT1 was mainly distributed in the membrane and PKM2 in the cytosol. Since they are housekeeping proteins, the increased expression of that proteins on microscopic imaging was not clear (Figure 16). However, serine phosphorylated PKM2 (S37) dramatically increased in co-cultured MCF7 cells compared to single culture cells (Figure 17). Interestingly phosphorylated PKM2 signals were observed mainly in nucleus as well as cytosol of MCF7 cell. Several studies reported that serine phosphorylation of PKM2 (S37) induces its nuclear localization and performs non-glycolytic functions such as gene transcriptional regulation, which, in turn, facilitates metabolic reprogramming in cancer cells (50,

51). In addition, we tried to confirm the correlation between EV uptake and increased PKM2 phosphorylation, increased expression of PKM2 and GLUT1. The EV signals were well visualized in cytosol of MCF7 cells co-cultured with MDA-MB-231-tdTomato (Figure 18).

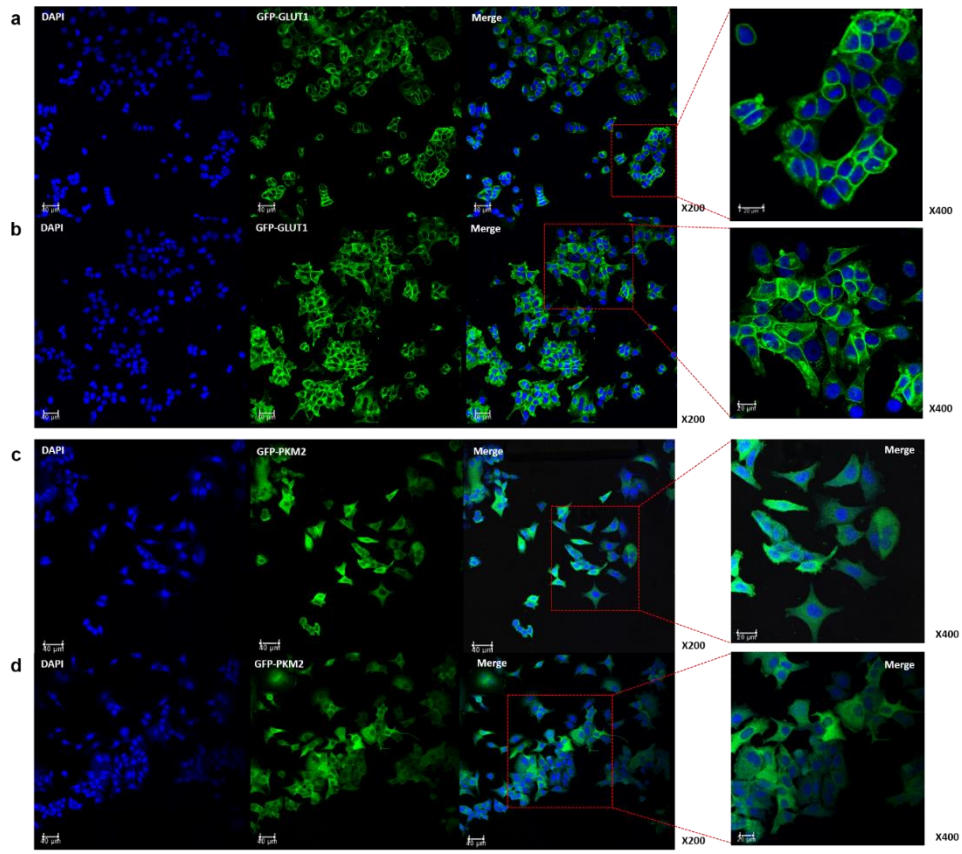

Figure 16. Expression pattern of PKM2 in the MCF7 cell after co-culture with MDA-MB-231 cell.

There was no clear change in GLUT1 (a-b) and PKM2 (c-d) expression in MCF7 cells after co-culture with MDA-MB-231 cells on fluorescence images.

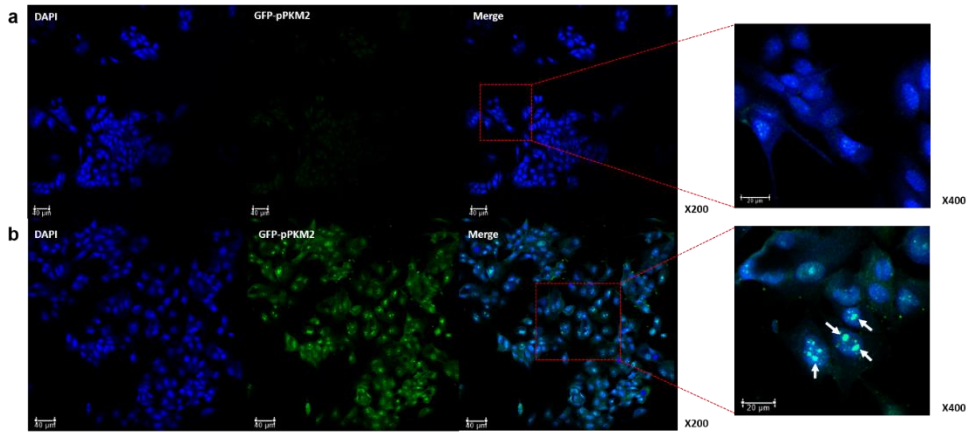

Figure 17. Increased phosphorylation of PKM2 in the MCF7 cell after co-culture with MDA-MB-231 cell.

Phosphorylation of PKM2 S37 revealed dramatic increase in co-cultured MCF7 cells (b) compared to single-cultured (a).

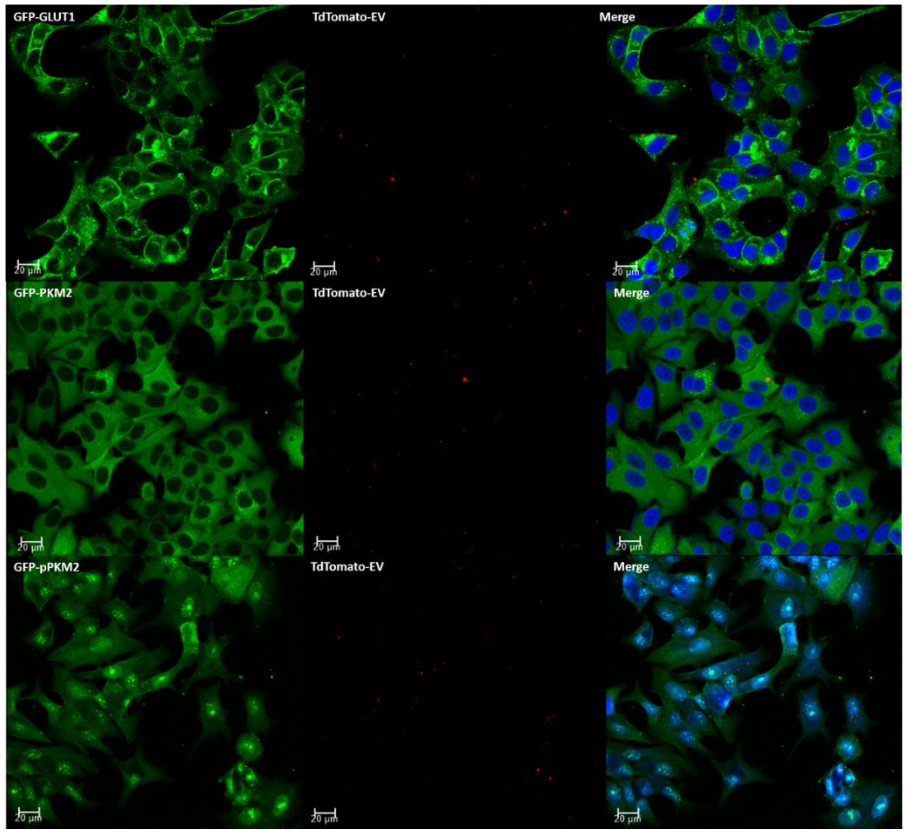

Figure 18. Visualized tdTomato EV signals inside MCF7 cells.

Td-Tomato signals suggesting EV were identified inside MCF7 cells together with expressed GLUT1 and PKM2, and phosphorylated PKM2.

Increased GLUT1 expression and PKM2 Y105 phosphorylation in co-cultured MCF7 cells

Western blot analyses also showed that expression of GLUT1 and PKM2 were increased in the co-cultured MCF7 cell compared to single-cultured one, although not statistically significant in PKM2. Tyrosine phosphorylation of PKM2 (Y105) was significantly increased in the co-cultured MCF7 cells, again suggesting that aerobic glycolysis was stimulated by co-culture with MDA-MB-231 cells (Figure 19). Especially, ratio of PKM2 phosphorylation to PKM2 was significantly increased in the co-cultured MCF7 cells, suggesting phosphorylation of PKM2 was a key stimulant for activated aerobic glycolysis (Figure 19c).

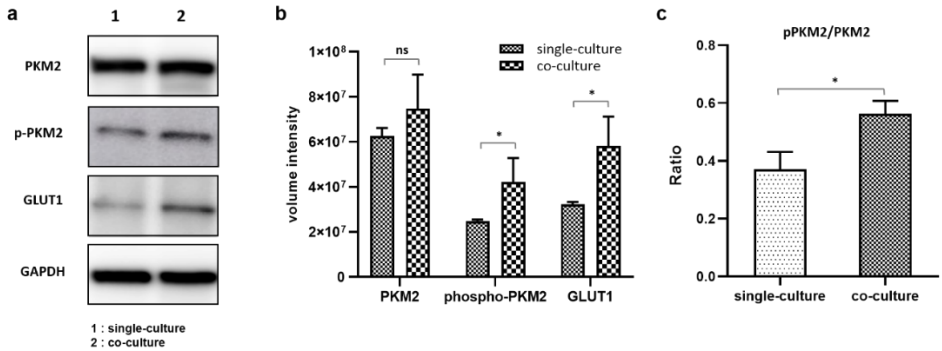

Figure 19. Western blotting to evaluate the expression of GLUT1, PKM2, and phosphorylation of PKM2

a, Results of expression level of GLUT1, PKM2, and phosphorylation of PKM2; b, Quantification of western blotting showed increased expression of GLUT1 and increased phosphorylation of PKM2 Y105, leading activation of aerobic glycolysis; c, Increased phosphorylation of PKM2 compared to expression of PKM2.

ns, not significant; *,P<0.05;

Inhibition of EV uptake prevented the activation of PKM2 phosphorylation in MCF7 cells

In the above results, the increase in FDG uptake of MCF7 co-cultured with MDA-MB-231 cells was inhibited by heparin, known to interfere with EV uptake. To evaluate the change of expression of glycolytic proteins by heparin, expression of GLUT1, PKM2 and phosphorylation of PKM2 were evaluated. In each cell, the expression of GLUT1 and PKM2 did not change much when determined visually. However, even though the same amount of cells were seeded, cell population of the heparin treated group showed a decrease, indicating that cell proliferation was reduced by inhibition of EV uptake (figure 20). In addition, phosphorylation of PKM2 was greatly suppressed, showing a similar pattern to that seen in single-cultured MCF7 cells (figure 21). That is, it can be considered that the effect of MDA-MB-231-derived EV disappeared due to inhibition of EV uptake. Therefore, it can be confirmed that MDA-MB-231-derived EVs induce aerobic glycolysis by activating phosphorylation of PKM2 and cell proliferation in the MCF7 cells.

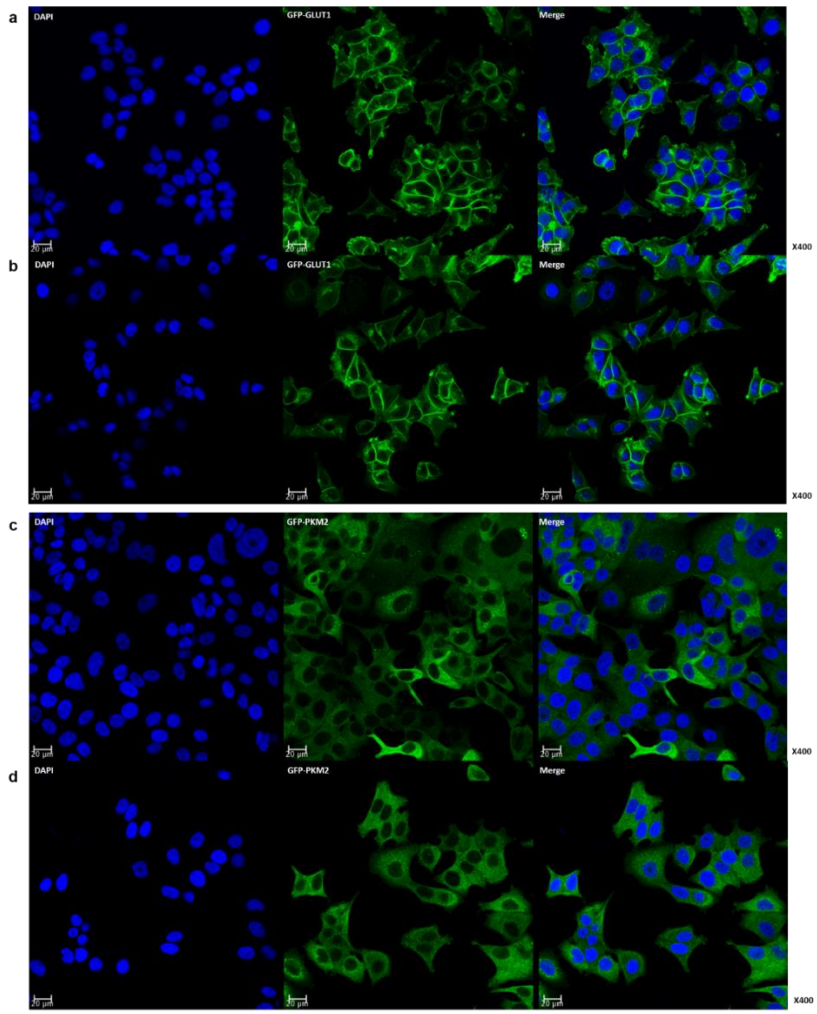

Figure 20. The expression pattern of GLUT1 and PKM2 after inhibiting EV uptake in co-culture MCF7 cell

The expression of GLUT1 and PKM2 after heparin treatment was not significantly changed, but cell proliferation was clearly increased. a, GLUT1 expression in co-cultured MCF7 cells; b, GLUT1 expression in co-cultured MCF7 cells with heparin; c, PKM2 expression in co-cultured MCF7 cells; d, PKM2 expression in co-cultured MCF7 cells with heparin.

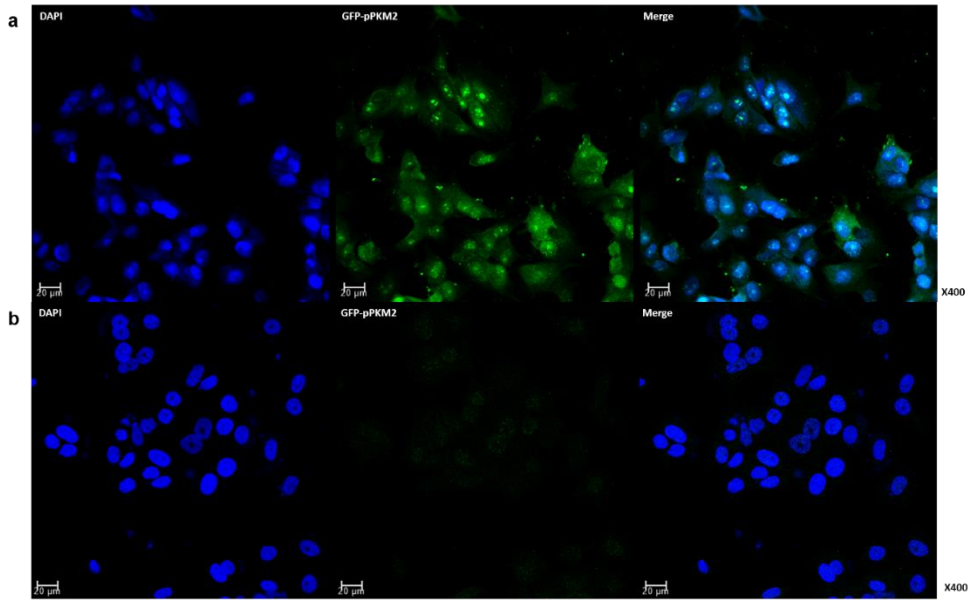

Figure 21. Suppressed PKM2 phosphorylation by inhibition of EV uptake.

PKM2 phosphorylation was suppressed to the level of single-cultured cells after heparin treatment in co-culture MCF7 cells. a, PKM2 phosphorylation in co-cultured MCF7 cells; b, PKM2 phosphorylation in co-cultured MCF7 cells with heparin.

Part III. Proteomic profiling of co-cultured MCF7 cells

Proteomic profiling of MCF7 co-cultured with MDA-MB-231 represent a shift to cells with aggressive phenotype.

Through the above experiments, we were able to confirm the role of EVs in regulating the glucose metabolism of recipient cells. To obtain a comprehensive perspective of the changes induced by MDA-MB-231 cell-derived EV, we determined proteome profiles of MCF7 cells co-cultured for 24h and 48h with MDA-MB-231 cells and single-cultured as a control. A comparative analysis between the single-cultured and co-cultured MCF7 cells identified 32 proteins after co-culture for 24h and 75 proteins for 48h, and except for duplicate value, showed that a total of 97 proteins were differentially expressed (Figure 22). ANOVA analysis of three groups identified five protein clusters according to expression pattern, two major clusters - number of 379 and 381- of them that had a consistent direction of expression were selected (Figure 23). According to GO term analysis using IPA, the proteins contained in cluster 379 were mainly classified into the following categories: regulation of cell communication, nucleobase-containing compound biosynthetic process, cellular response to organic substance, positive regulation of gene expression and so on. On the other hand, proteins in cluster 381 mainly represented gene ontology associated with cell dedifferentiation, such as cell morphogenesis and regulation of cell differentiation (Table 1). Protein-protein interaction for differentially expression proteins was visualized using STRING analysis, and three main interactive clusters - up-regulated of nucleobase-containing compound

biosynthetic process, and down-regulated cell morphogenesis and regulation of cell differentiation - were displayed (Figure 24).

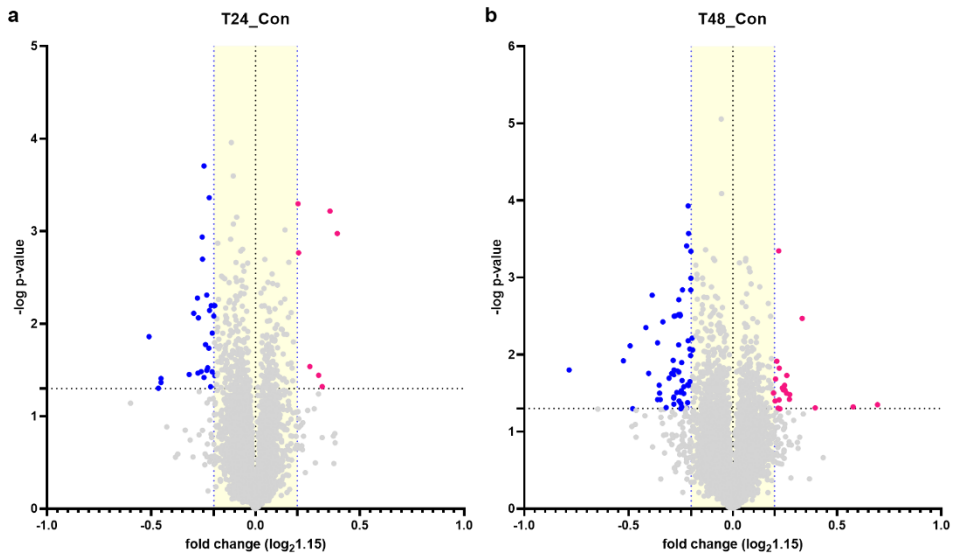

Figure 22. Volcano plotting described differentially expressed proteins in the MCF7 cell co-culture with MDA-MB-231 (-log p-value>1.3 and fold change≥1.15)

A comparative analysis between the single-cultured and co-cultured MCF7 cells identified 32 differentially expressed proteins after co-culture for 24h and 75 proteins for 48h. Excluding the duplicate value, a total of 97 proteins were differentially expressed.

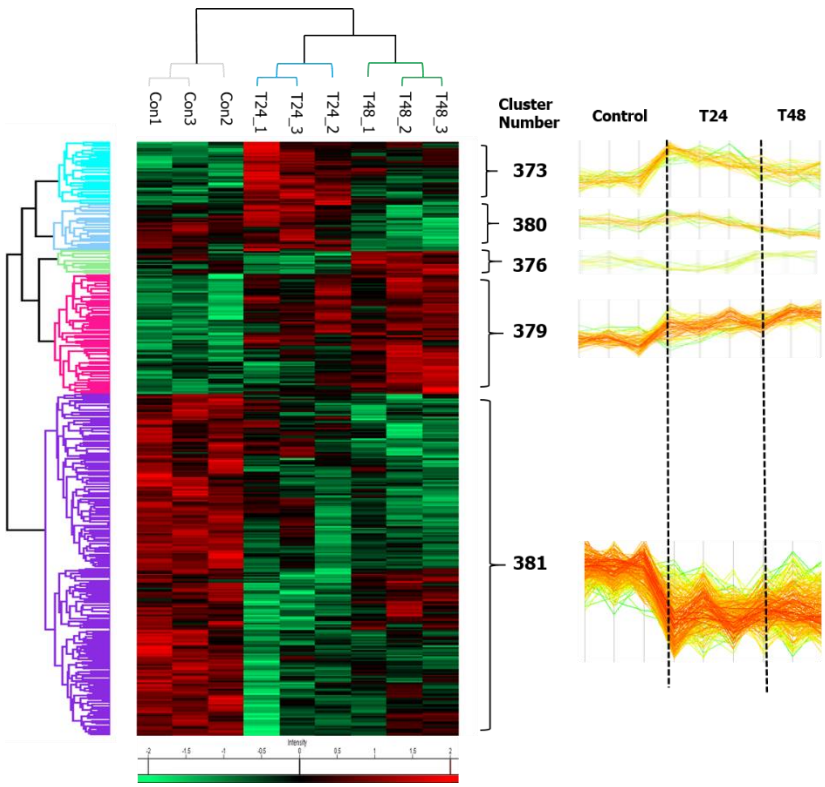

Figure 23. Hierarchical clustering represented five clusters

There are five major clusters, and of them, we noted the major two cluster (#379 and #381) with consistent direction in expression.

	GO Term	P-value	Genes	Fold Enrichment
Up-regulated	Protein modification by small protein conjugation	0.008839	CDCA8, NMI, N4BP1, BTRC, UBA7, BIRC5, FKBP1A, CBFB, SPOP, TRAF3	2.760462
	Positive regulation of metabolic process	0.014763	SREBF1, RET, MYO6, NMI, BTRC, ADCY5, TPX2, FKBP1A, WHSC1, CBFB, ARHGEF11, NRIP1, NOTCH3, ITGA6, IRF7, NFAT5, AKAP5, CCS, FOXC1, ABL2, NCOR2	1.684768
	Nucleobase-containing compound biosynthetic process	0.015722	SREBF1, RET, NMI, MYO6, ADCY5, BTRC, ZNF48, UBA7, WHSC1, BIRC5, CBFB, ARHGEF11, NRIP1, NOTCH3, NOTCH2, ITGA6, IRF7, PARP14, TOP3A, NFAT5, AKAP5, THOC7, FOXC1, GUK1, NCOR2, TRAF3, ZNF768	1.517335
	Positive regulation of transcription, DNA-templated	0.018126	NOTCH3, SREBF1, RET, MYO6, ITGA6, BTRC, IRF7, NFAT5, FOXC1, CBFB, NRIP1, ARHGEF11	2.178084
Down-regulated	Cell morphogenesis involved in differentiation	2.82E-06	COBL, HRAS, ACTN4, PDLIM5, PREX1, BAIAP2, ACTN1, BASP1, PALLD, LATS2, FOXP1, FLNA, NUMBL, TGFB2, CORO1C, GLIPR2, CDC42, UNC13D, MACF1, SIPA1L1, CAMK2B, BCL9L, ZFPM1, RAPGEF2, OLFM1, GBP1	2.918276
	Regulation of cell differentiation	0.004287	XRCC5, COBL, PDLIM7, PDLIM5, PREX1, IL18, PDCD4, TGFB2, CDC42, GLIPR2, MACF1, PER2, BCL9L, CAMK2B, RAPGEF2, EHD2, OLFM1, ACTN4, BAIAP2, PTBP1, ARNTL, FOXP1, FLNA, NUMBL, CORO1C, UFL1, UNC13D, SIPA1L1, ZFPM1, KDM4A, GBP1	1.696924
	Regulation of apoptotic process	0.039927	TXNIP, HRAS, HTATIP2, AIFM2, ACTN4, ERBB3, VIL1, FHL2, ACTN1, PAWR, PDCD4, LATS2, FOXP1, FLNA, TGFB2, ATF6, FIS1, CDC42, SON, AKT1S1, SOS2, CAMK2D, DEPTOR, RAPGEF2, PDCD6	1.509246
	Signal transduction involved in mitotic cell cycle checkpoint	0.038111	CNOT8, RBL2, PPP2R5C, TFDP2	5.366207

Table 1. GO term analysis

The proteins contained in cluster 379 were up-regulated with longer incubation time. These are mainly proteins involved in protein modification, positive regulation of metabolic process, nucleobase-containing compound biosynthetic process, and positive regulation of gene expression. On the other hand, the cluster 381 consisted mainly of proteins related to cell dedifferentiation, such as cell morphogenesis and regulation of cell differentiation.

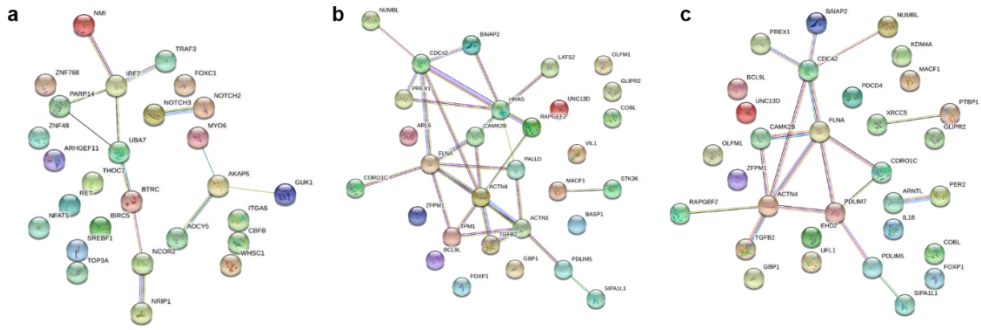

Figure 24. Visualization of protein-protein interactions of the differentially expressed proteins in MCF7 cells using STRING analysis.

It formed several major clusters – Nucleobase-containing compound biosynthetic process (a), cell morphogenesis (b), and regulation of cell differentiation (c). Lines represented interactions between proteins and thickness denoted the confidence level associated with each interaction.

Differential expression of proteins involved in Epithelial to Mesenchymal transition

Epithelial-mesenchymal transition (EMT) is the most crucial feature of metastatic cancers which stimulates nuclear translocation of PKM2 to inhibit E-cadherin activity. Thus, PKM2-mediated downregulation of E-cadherin lead to the loss of epithelial cell-cell adhesion, and subsequently promotes the invasion and metastasis. In our data, markers of the epithelial phenotypes such as the tight junction protein ZO-1 (TJP1) and protocadherin beta-2 (PCDHB2) were reduced in MCF7 cells co-cultured with MDA-MB-231 for the first 24 hours. And then, important proteins such as ETS-related transcription factor (ELF3), transcription factor SOX-9 (SOX9), ras-related C3 botulinum toxin substrate 3 (RAC3), Caveolin-1 (CAV1), and Dickkopf-related protein 1 (DKK1), which were well known as EMT driver, were differentially expressed in co-cultured MCF7 cells for 48 hours (figure 25).

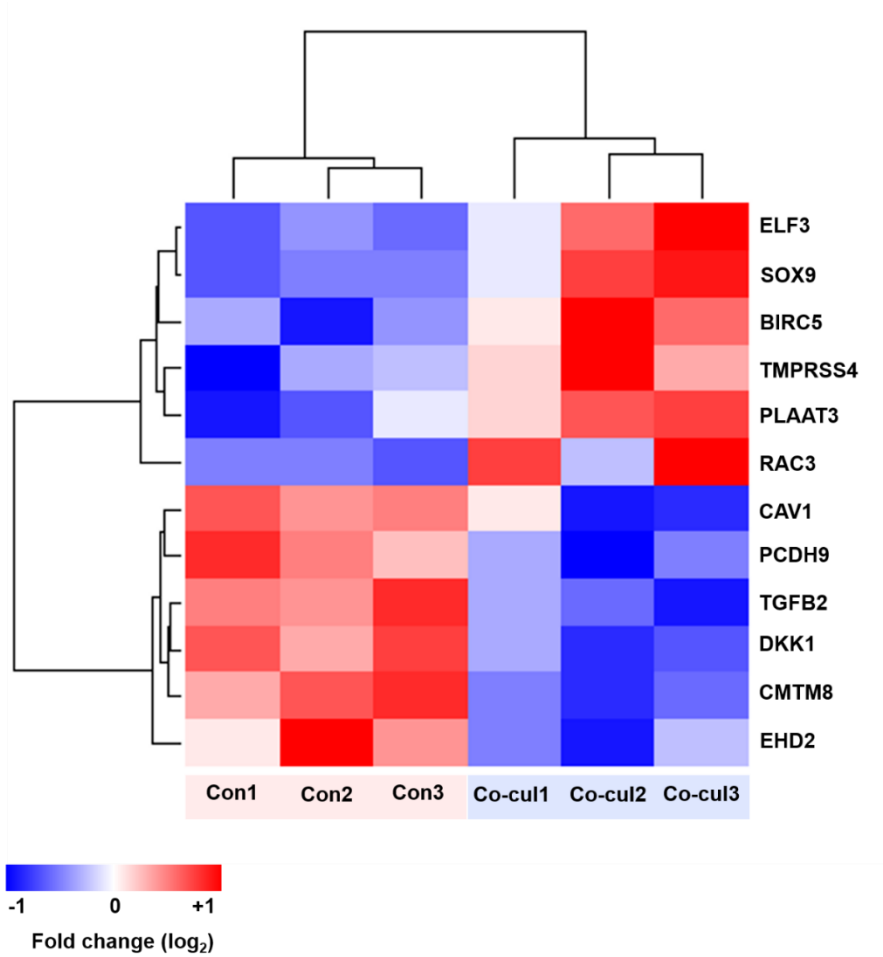

Figure 25. Differential expression of EMT-related proteins in MCF7 after co-culture with MDA-MB-231

A number of proteins associated to EMT were differentially expressed in the MCF7 cells co-cultured for 48 hours compared to single-cultured.

Con, control cell (single-culture MCF7 cell); Co-cul, MCF7 cell co-cultured with MDA-MB-231

MDA-MB-231-derived EVs have proteins related to PKM2 phosphorylation as well as glycolysis.

Next, we examined proteome profiles of EVs from MDA-MB-231 cells to find the key molecules that led to these changes, resulting in the identification of a total of 856 proteins in biological triplicate. We compared the 856 proteins with previously published data in Vesiclepedia databases. Our results indicated overlaps of 823 (96%) and 685 (80%) of proteins among total identified EV and MDA-MB-231 cell-derived EV in Vesiclepedia database, respectively (Figure 26). To investigate the biologic function of the identified proteins, GO analysis was conducted. Proteins were sorted into categories according to their ontology as determined from their GO annotation terms. The annotated biologic processes of the proteins revealed enrichment of EV-associated proteins related to RNA binding, translational initiation, and post-translational protein modification (Figure 27). In addition, analysis of the KEGG pathway of EV proteins revealed total 360 signal pathways, and there were 36 significant pathways consisting of a considerable number of proteins. Among them were glycolysis/gluconeogenesis, pyruvate metabolism, and PI3K-Akt signaling pathways (Figure 28). PI3K signaling pathway contains proteins such as EGFR, ERBB2, and MAPK1, which are well known for phosphorylating PKM2. Therefore, we suggest the possibility that the EGFR, ERBB2, and MAPK1, the cargo proteins of EV, have phosphorylated PKM2 and resulted in activated aerobic glycolysis and cell proliferation.

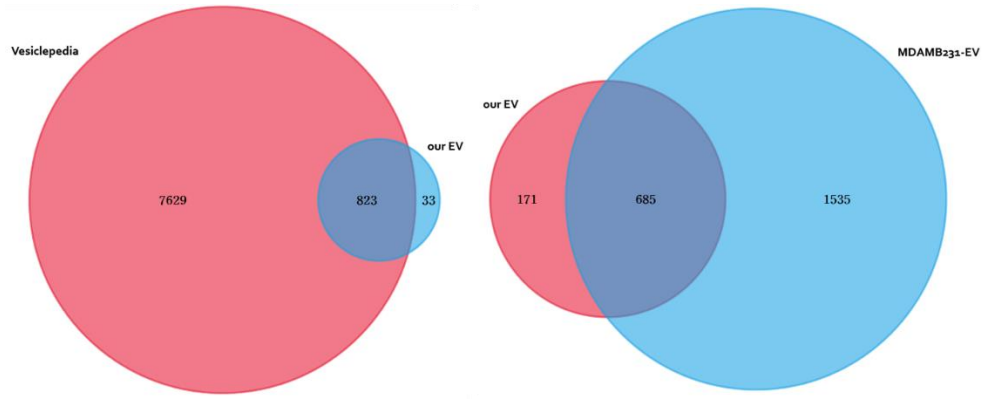

Figure 26. Venn diagram describing the matched proteins with total EV and MDA-MB-231 EV database from Vesiclepedia.

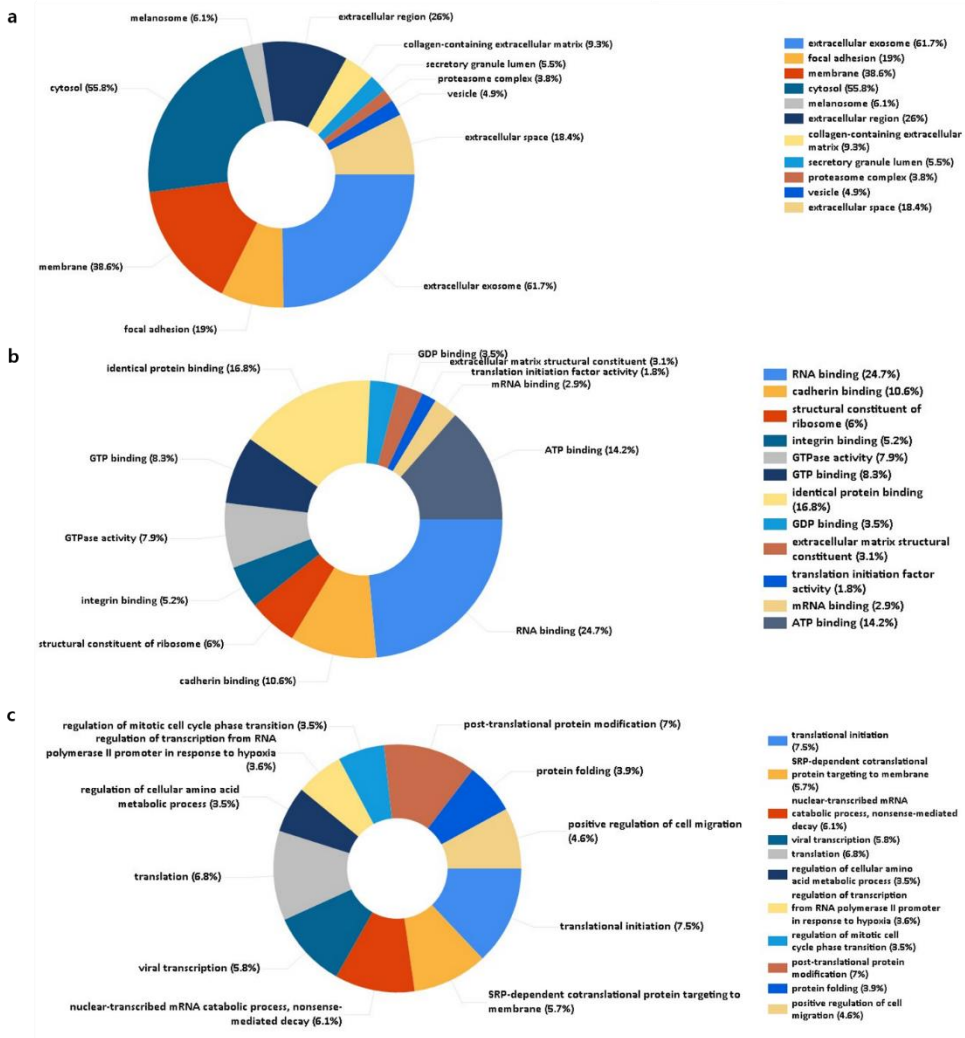

Figure 27. The GO analysis of the 856 proteins identified in the MDA-MB-231-derived EVs.

The GO analysis of the 856 proteins identified in the MDA-MB-231-derived EVs. a, cellular component; b, molecular function; c, Biologic process

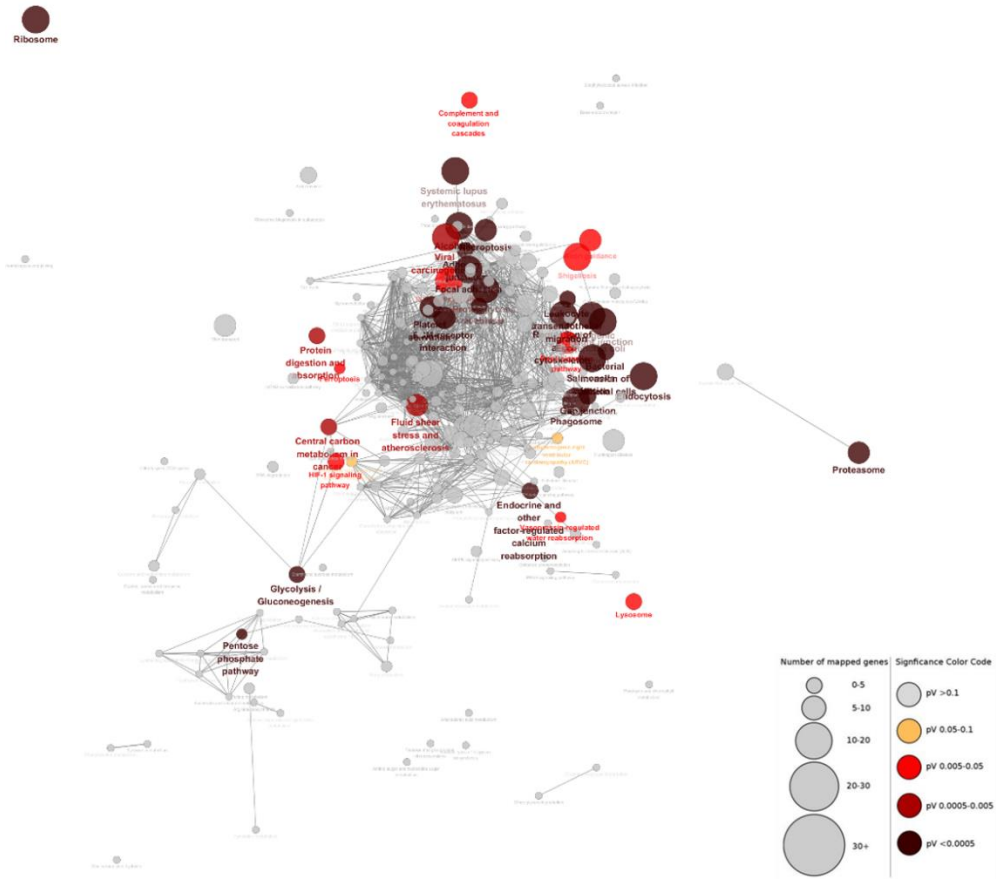

Figure 28. KEGG pathway analysis of MDA-MB-231-derived EVs.

Several important pathways related to aerobic glycolysis and cell proliferation have been found: Glycolysis/gluconeogenesis, Pyruvate metabolism and PI3K-Akt signaling pathway.

Pathway	Genes
PI3K-Akt signaling pathway	COL1A1, COL1A2, COL2A1, COL4A1, COL4A2, COL4A5, COL6A1, COL6A2, COL6A3, **EGFR**, EPHA2, **ERBB2, ERBB4**, FN1, GNB1, GNB2, GNB3, GNB4, GNG12, GNG5, HRAS, HSP90AA1, HSP90AB1, IGF2, ITGA2, ITGA2B, ITGA3, ITGA6, ITGAV, ITGB1, ITGB3, KRAS, LAMA3, LAMA5, LAMB1, LAMB2, LAMB4, LAMC1, **MAPK1**, NRAS, PDGFC, RAC1, RELN, RPS6, THBS1, THBS2, THBS3, THBS4, TNC, VWF, YWHAB, YWHAE, YWHAG, YWHAH, YWHAQ, YWHAZ
Glycolysis/Gluconeogenesis	ADH5, ALDH7A1, ALDH9A1, ALDOA, ALDOC, BPGM, ENO1, ENO2, ENO3, GAPDH, GAPDHS, GPI, LDHA, LDHAL6A, LDHB, LDHC, PFKL, PFKM, PFKP, PGAM1, PGAM2, PGK1, PGK2, PKLR, PKM, TPI1
Pyruvate metabolism	ACOT12, ALDH7A1, ALDH9A1, FH, LDHA, LDHAL6A, LDHB, LDHC, MDH1, PKLR, PKM

Table 2. Genes involved in major pathways related to aerobic glycolysis and cell proliferation.

We have found important functional pathways consisting of genes of significant level in constructing their pathway, such as glycolysis and PI3K signaling pathway. PI3K signaling pathway contains a number of proteins -EGFR, ERBB2, and MAPK1- well known for phosphorylating PKM2.

Discussion

Cell-to-cell communication is an essential process for cell biology and function of in vivo, and many elements are organically connected to facilitate theses interactions. Among them, the most recent thing that has attracted great attention is the extracellular vesicles. Extracellular vesicles comprise a heterogeneous population of membrane vesicles of various origins. Their size may vary (typically between 50 nm and 500 nm, but they can be even larger, measuring 1-10 μm). Over the past two decades, extracellular vesicles have been named based on their origin (cell type), size, morphology and cargo content but can now be classified into two distinct classes: exosomes and microvesicles (9). There are a few articles that evaluated the role of EVs modulating glucose metabolism in recipient cells (2, 52). But, most studies focus primarily on the relationship between cancer and stromal cells, so there is little research on the communication of cancer cells through EVs. So we investigated changes of aerobic glycolysis, the hallmark of cancer, in order to see the interaction between cancer cells though cancer cell-derived EVs.

Our findings suggest that MDA-MB-231-derived EVs instigated phosphorylation of PKM2, resulted in increased aerobic glycolysis and cell proliferation, that is, transformed MCF7 cells more aggressively. These imply the possibility of interaction between subclones within a tumor in terms of cell-to-cell communication and tumor heterogeneity. There are a few studies dealing with the interaction between cancer cells in a tumor (53-55). Rak et al., reported that oncogenic receptor tyrosine kinase, EGFRvIII, were transferred to EGFR-negative

endothelial cells (HUVECs) and A431 cells expressing only wtEGFR through microvesicles derived from EGFRvIII-positive glioblastoma cells, resulting in activation of downstream signaling pathway such as MAPK and Akt (37). In a similar way, in our result, MCF7 co-cultured with more aggressive subtype, MDA-MB-231 cells, revealed dramatically increased glucose uptake compared to baseline uptake level. EVs isolated from MDA-MB-231 cells also had a similar effect, although not as effective as co-cultured. Increased cellular proliferation and lactate production accompanied by increased glucose uptake are signified to be caused by activated aerobic glycolysis rather than oxidative phosphorylation. Therefore, it can be inferred that these have been wrought by a special cargo of MDA-MB-231-derived EVs. EV-deprived conditioned media from MDA-MB-231 and HFF cells also produced a significant glucose uptake in the recipient MCF7 cells, although not as much as EVs, which is explained by the high volume of substances including growth factors secreted from cells. Given the significant difference between the effects of EV and CM, this is a result supporting the activation of glucose metabolism by EV. Further study should be conducted to identify specific elements inside the EV.

It has been well established that tumor cells have elevated rates of glucose uptake and high lactate production in despite of the presence of oxygen, known as aerobic glycolysis (56). Glucose-metabolizing enzymes, including pyruvate kinase, are often upregulated in cancer cells (57, 58). PKM2 has two isoforms, tetrameric and dimeric forms, and exhibits a high level of catalysis when protein is in a tetrameric state but provides a growth advantage in a dimeric state (59). PKM2

convert to a dimeric form when Y105 is phosphorylated, and the dimeric form of PKM2 has low affinity for the precursor, PEP, leading to the aerobic glycolysis with increased lactate production (60). Immunoblotting analyses showed that GLUT1 expression increased in the co-cultured MCF7 compared to control MCF7. Although PKM2 expression itself did not show significant change in the co-cultured MCF7, phosphorylation of PKM2 suggesting conversion to oncogenic PKM2 was increased in the co-cultured MCF7.

Unlike tyrosine phosphorylation of PKM2 that principally modulates its glycolytic function, serine phosphorylation of PKM2 induces its nuclear localization (50, 51, 61) and is essential for tumorigenesis (62). Fluorescence images stained with phospho-PKM2-S37 antibody described increased signals in nucleus with relatively week but clear uptake in cytosol of co-cultured MCF7 cells. To be exactly, the main signals seems to be located in nucleolus. The nucleolus is a distinct subnuclear compartment and primarily associated with ribosome biogenesis. However, several lines of evidence represent it has additional functions, such as regulation of mitosis, cell-cycle progression and proliferation (63). The S37 phosphorylated PKM2 assists the transcriptional activation of signal transducer and activator of transcription 5 (STAT5) to facilitate the expression of different genes such as cyclin D1, c-Myc, glucose transporter 1 (GLUT1), lactate dehydrogenase A (LDHA), and PKM2, all essential for tumor cell metabolic reprogramming and proliferation (29, 50, 51). Therefore, nuclear localization of S37 phosphorylated PKM2 stimulated in co-cultured MCF7 cells supports that MDA-MB-231-derived EVs lead conversion of MCF7 cells to more aggressive cancer cell. In addition, after adding heparin that

interfered with the EV uptake of MCF7 cells, activation of S37 phosphorylation in co-cultured MCF7 cell was suppressed. Cell proliferation was also reduced in the heparin treated group. This once again reveals the role of MDA-MB-231-derived EVs, indicating the need to uncover the major substances inside the EV that caused this reaction. What's interesting is that the S37 phosphorylation signal was feeble in a single cultured MCF7 cells, compared with very strong S37 phosphorylation in single-cultured MDA-MB-231 cells. This is probably related to the less proliferative nature of MCF7 cells, and further research is needed.

MDA-MB-231 cells represented different patterns in expression of GLUT1 and phosphorylation of PKM2. Unlike MCF7 cells, most of the GLUT1 proteins was located in the cytosol like granules. It can be interpreted that the highly expressed GLUT1 proteins are in the endoplasmic reticulum or Golgi apparatus. In addition, S37 phosphorylation of PKM2 in MDA-MB-231 cells was highly activated and located throughout the cell as well as nucleus (figure 29). Although both are breast cancer cells, these differences between MCF7 and MDA-MB-231 cells seems to be due to a fundamental heterogeneous nature. However, by MDA-MB-231-derived-EVs, the pattern of PKM2 phosphorylation in MCF7 cells was changed similarly to MDA-MB-231 cells. Therefore, it can be a clue to the transfer of characteristic substances by EV between different cells.

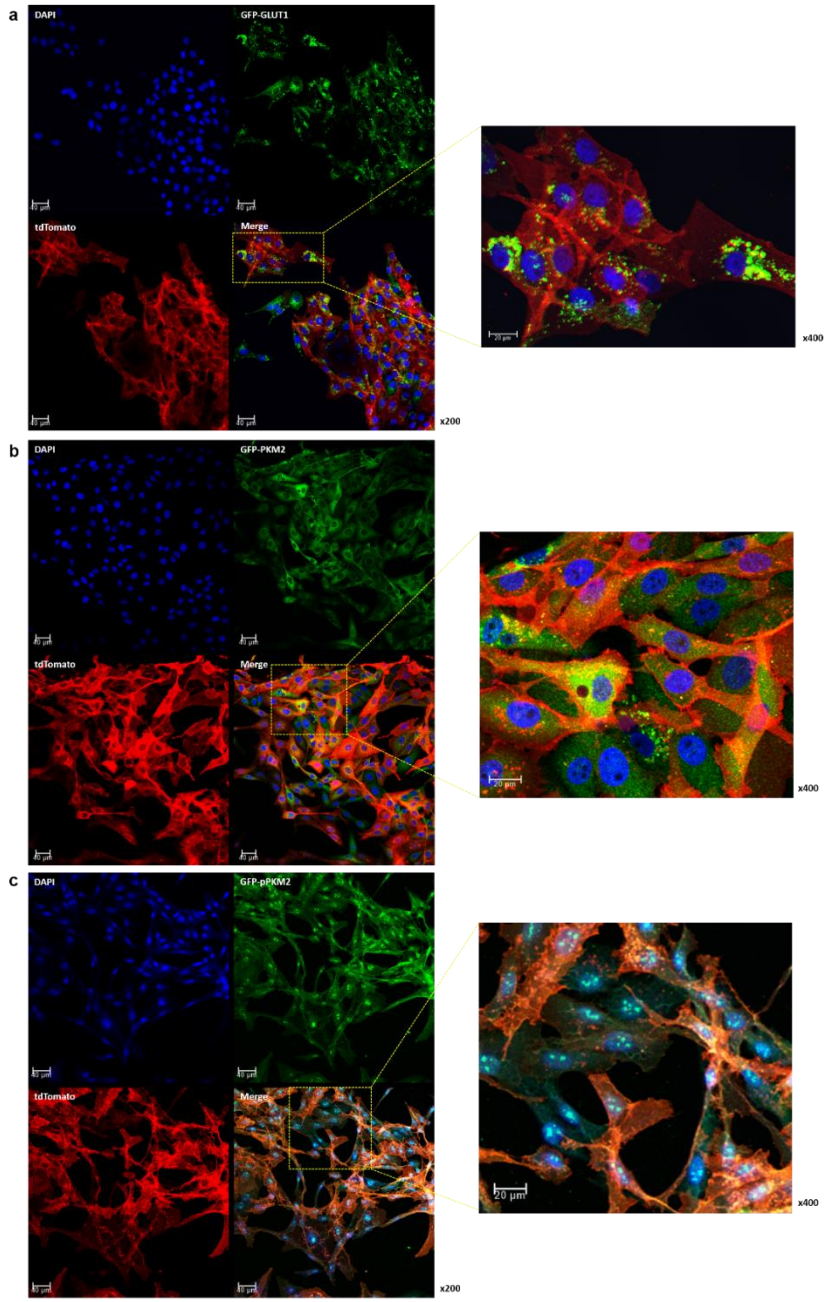

Figure 29. Expression of GLUT1 (a), PKM2 (b), and S37 phosphorylation of PKM2 (c) in MDA-MB-231-tdTomato cells

Proteomics analysis results revealed that a total number of 97 proteins were differentially expressed in MCF7 co-cultured with MDA-MB-231 compared to single-cultured MCF7 cells. GO analysis showed that cell differentiation decreased, whereas gene expression and translation increased in the co-cultured MCF7 cells. This is in line with the results of FDG uptake test, immunoblot and immunostaining, which show increased glucose uptake and phosphorylation of PKM2. In addition, a number of EMT-related proteins existed among 97 differentially expressed proteins. Marker protein of epithelial phenotypes such as TJP1 and PCDHB2 began to decrease in expression in co-cultured MCF7 cell of 24 hours, and after co-culture of 48 hours, the expression of proteins such ELF3, SOX9, RAC3, DKK1, and CAV1, known as EMT driver, also increased or decreased according to their role. Considering the characteristics of the MDA-MB-231 cell of the claudin-low type, which is enriched in EMT features, it can be interpreted that the EV derived from MDA-MB-231 delivered these characteristics to the MCF7 cell.

As mentioned above, nuclear PKM2 is well known to act as a transcription factor, contributing to the expression of several proteins involved in cell proliferation. Furthermore, it is also known to interact with TGF-β-induced factor homeobox 2 (TGIF2) and to repress E-cadherin expression during EMT, which plays a critical role in the transition to mesenchymal phenotype of cancer cell (64, 65). Therefore, the special cargo protein in EV not only activated aerobic glycolysis by phosphorylating PKM2 but also induced nuclear transfer of PKM2 to result in EMT occurring.

A number of significant KEGG pathways were identified in the 856 protein analysis identified in MDA-MB-231-derived EVs, where glycolysis and PI3K-Akt signaling pathways were present. PI3K-Akt signaling pathway promotes metabolism, proliferation, cell survival, and growth and contains a number of proteins such as EGFR, ERBB2, and MAPK1, associated with their function. ERBB2, one of oncogenic tyrosine kinases that are frequently activated in breast cancers can phosphorylate PKM2 at Y105 (66). EGFR and MAPK1 are also famous oncogenic kinases and have the ability to phosphorylate PKM2 at S37 (50, 51). Therefore, we suggest the possibility that the EGFR, ERBB2, and MAPK1, the cargo proteins of EV, have phosphorylated PKM2 and resulted in activated aerobic glycolysis and cell proliferation, even transition to mesenchymal phenotype in the MCF7 cells co-cultured with MDA-MB-231 cells (figure 30).

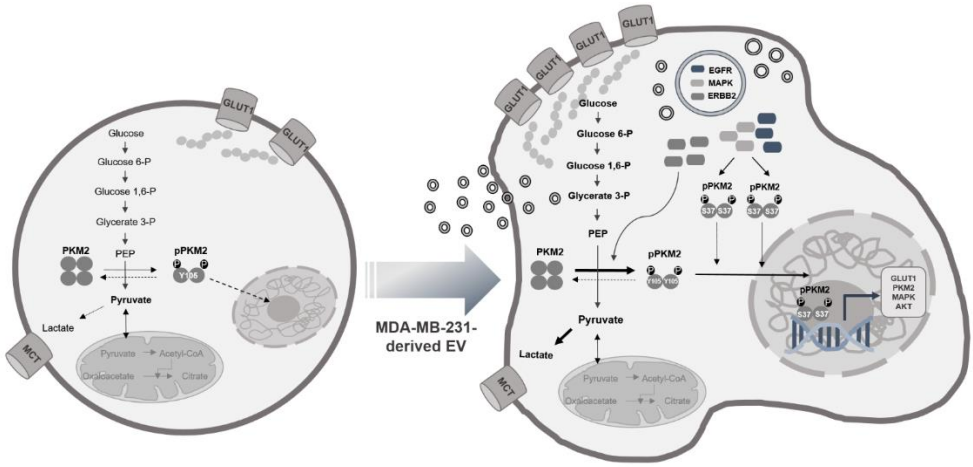

Figure 30. A schematic diagram representing the role of MDA-MB-231-derived EV in MCF7 cell.

Left, MCF7 cell: PKM2 proteins are partially phosphorylated at Y105 and form dimer, but phosphorylation at S37 hardly occurs; Right, MCF7 cell co-cultured with MDA-MB-231 cell: EVs derived from MDA-MB-231 cell transferred their cargo proteins such as ERBB2, EGFR and MAPK1 which can phosphorylate PKM2 at Y105 and S37 to MCF7 cell. Y105 phosphorylation of PKM2 activated aerobic glycolysis, which resulted in increased glucose uptake and lactate production. S37 phosphorylation induced nuclear translocation of PKM2 and resulted in increased expression of several proteins involved in glycolysis and cell proliferation.

Conclusion

EVs originated from MDA-MB-231 cell have upregulated aerobic glycolysis by inducing phosphorylation of PKM2 in the MCF7 cell, which finally made dedifferentiation and cellular proliferation. Therefore, given the ability of EVs originated from MDA-MB-231 cell to cause tumor progression of other cancer cell, we note the potential impact of aggressive cancer cells on other cancer cells nearby in terms of intratumor heterogeneity. This impact may be caused by an intermediary called EVs.

References

1. Chiodoni C, Di Martino MT, Zazzeroni F, Caraglia M, Donadelli M, Meschini S, et al. Cell communication and signaling: how to turn bad language into positive one. Journal of experimental & clinical cancer research : CR. 2019;38(1):128.
2. Fong MY, Zhou W, Liu L, Alontaga AY, Chandra M, Ashby J, et al. Breast-cancer-secreted miR-122 reprograms glucose metabolism in premetastatic niche to promote metastasis. Nature cell biology. 2015;17(2):183-94.
3. Brucher BL, Jamall IS. Cell-cell communication in the tumor microenvironment, carcinogenesis, and anticancer treatment. Cellular physiology and biochemistry : international journal of experimental cellular physiology, biochemistry, and pharmacology. 2014;34(2):213-43.
4. Dehne N, Mora J, Namgaladze D, Weigert A, Brune B. Cancer cell and macrophage cross-talk in the tumor microenvironment. Current opinion in pharmacology. 2017;35:12-9.
5. Conti I, Varano G, Simioni C, Laface I, Milani D, Rimondi E, et al. miRNAs as Influencers of Cell-Cell Communication in Tumor Microenvironment. Cells. 2020;9(1).
6. Bian X, Xiao YT, Wu T, Yao M, Du L, Ren S, et al. Microvesicles and chemokines in tumor microenvironment: mediators of intercellular communications in tumor progression. Molecular cancer. 2019;18(1):50.
7. Becker A, Thakur BK, Weiss JM, Kim HS, Peinado H, Lyden D. Extracellular Vesicles in Cancer: Cell-to-Cell Mediators of Metastasis. Cancer cell. 2016;30(6):836-48.
8. Muralidharan-Chari V, Clancy JW, Sedgwick A, D'Souza-Schorey C. Microvesicles: mediators of extracellular communication during cancer progression. Journal of cell science. 2010;123(Pt 10):1603-11.
9. van Niel G, D'Angelo G, Raposo G. Shedding light on the cell biology of extracellular vesicles. Nature reviews Molecular cell biology. 2018;19(4):213-28.
10. Maia J, Caja S, Strano Moraes MC, Couto N, Costa-Silva B. Exosome-Based Cell-Cell Communication in the Tumor Microenvironment. Frontiers in cell and developmental biology. 2018;6:18.

11. Raposo G, Stoorvogel W. Extracellular vesicles: exosomes, microvesicles, and friends. The Journal of cell biology. 2013;200(4):373-83.
12. Zaborowski MP, Balaj L, Breakefield XO, Lai CP. Extracellular Vesicles: Composition, Biological Relevance, and Methods of Study. Bioscience. 2015;65(8):783-97.
13. Martins VR, Dias MS, Hainaut P. Tumor-cell-derived microvesicles as carriers of molecular information in cancer. Current opinion in oncology. 2013;25(1):66-75.
14. McAllister SS, Weinberg RA. The tumour-induced systemic environment as a critical regulator of cancer progression and metastasis. Nature cell biology. 2014;16(8):717-27.
15. S ELA, Mager I, Breakefield XO, Wood MJ. Extracellular vesicles: biology and emerging therapeutic opportunities. Nature reviews Drug discovery. 2013;12(5):347-57.
16. Gyorgy B, Hung ME, Breakefield XO, Leonard JN. Therapeutic applications of extracellular vesicles: clinical promise and open questions. Annual review of pharmacology and toxicology. 2015;55:439-64.
17. Garcia-Manrique P, Matos M, Gutierrez G, Pazos C, Blanco-Lopez MC. Therapeutic biomaterials based on extracellular vesicles: classification of bio-engineering and mimetic preparation routes. Journal of extracellular vesicles. 2018;7(1):1422676.
18. Sahebi R, Langari H, Fathinezhad Z, Bahari Sani Z, Avan A, Ghayour Mobarhan M, et al. Exosomes: New insights into cancer mechanisms. Journal of cellular biochemistry. 2020;121(1):7-16.
19. Ma Z, Cui X, Lu L, Chen G, Yang Y, Hu Y, et al. Exosomes from glioma cells induce a tumor-like phenotype in mesenchymal stem cells by activating glycolysis. Stem cell research & therapy. 2019;10(1):60.
20. Wang B, Wang X, Hou D, Huang Q, Zhan W, Chen C, et al. Exosomes derived from acute myeloid leukemia cells promote chemoresistance by enhancing glycolysis-mediated vascular remodeling. Journal of cellular physiology. 2019;234(7):10602-14.
21. Shu S, Yang Y, Allen CL, Maguire O, Minderman H, Sen A, et al. Metabolic reprogramming of stromal fibroblasts by melanoma exosome microRNA favours

a pre-metastatic microenvironment. Scientific reports. 2018;8(1):12905.
22. Warburg O. On the origin of cancer cells. Science (New York, NY). 1956;123(3191):309-14.
23. Gatenby RA, Gillies RJ. Why do cancers have high aerobic glycolysis? Nature reviews Cancer. 2004;4(11):891-9.
24. Kim JW, Dang CV. Cancer's molecular sweet tooth and the Warburg effect. Cancer research. 2006;66(18):8927-30.
25. Liu F, Ma F, Wang Y, Hao L, Zeng H, Jia C, et al. PKM2 methylation by CARM1 activates aerobic glycolysis to promote tumorigenesis. Nature cell biology. 2017;19(11):1358-70.
26. Dong G, Mao Q, Xia W, Xu Y, Wang J, Xu L, et al. PKM2 and cancer: The function of PKM2 beyond glycolysis. Oncology letters. 2016;11(3):1980-6.
27. Wong N, Ojo D, Yan J, Tang D. PKM2 contributes to cancer metabolism. Cancer letters. 2015;356(2 Pt A):184-91.
28. Israelsen WJ, Vander Heiden MG. Pyruvate kinase: Function, regulation and role in cancer. Seminars in cell & developmental biology. 2015;43:43-51.
29. Yang W, Lu Z. Pyruvate kinase M2 at a glance. Journal of cell science. 2015;128(9):1655-60.
30. Christofk HR, Vander Heiden MG, Harris MH, Ramanathan A, Gerszten RE, Wei R, et al. The M2 splice isoform of pyruvate kinase is important for cancer metabolism and tumour growth. Nature. 2008;452(7184):230-3.
31. Beinat C, Alam IS, James ML, Srinivasan A, Gambhir SS. Development of [(18)F]DASA-23 for Imaging Tumor Glycolysis Through Noninvasive Measurement of Pyruvate Kinase M2. Molecular imaging and biology : MIB : the official publication of the Academy of Molecular Imaging. 2017;19(5):665-72.
32. Beinat C, Patel CB, Haywood T, Shen B, Naya L, Gandhi H, et al. Human biodistribution and radiation dosimetry of [(18)F]DASA-23, a PET probe targeting pyruvate kinase M2. European journal of nuclear medicine and molecular imaging. 2020.
33. Beinat C, Patel CB, Xie Y, Gambhir SS. Evaluation of Glycolytic Response to Multiple Classes of Anti-glioblastoma Drugs by Noninvasive Measurement of Pyruvate Kinase M2 Using [(18)F]DASA-23. Molecular imaging and biology : MIB : the official publication of the Academy of Molecular Imaging. 2019.

34. Witney TH, James ML, Shen B, Chang E, Pohling C, Arksey N, et al. PET imaging of tumor glycolysis downstream of hexokinase through noninvasive measurement of pyruvate kinase M2. Science translational medicine. 2015;7(310):310ra169.
35. Wang X, Zhang F, Wu XR. Inhibition of Pyruvate Kinase M2 Markedly Reduces Chemoresistance of Advanced Bladder Cancer to Cisplatin. Scientific reports. 2017;7:45983.
36. Chen J, Xie J, Jiang Z, Wang B, Wang Y, Hu X. Shikonin and its analogs inhibit cancer cell glycolysis by targeting tumor pyruvate kinase-M2. Oncogene. 2011;30(42):4297-306.
37. Su Q, Luo S, Tan Q, Deng J, Zhou S, Peng M, et al. The role of pyruvate kinase M2 in anticancer therapeutic treatments. Oncology letters. 2019;18(6):5663-72.
38. Yeo SK, Guan JL. Breast Cancer: Multiple Subtypes within a Tumor? Trends in cancer. 2017;3(11):753-60.
39. Yates LR, Gerstung M, Knappskog S, Desmedt C, Gundem G, Van Loo P, et al. Subclonal diversification of primary breast cancer revealed by multiregion sequencing. Nature medicine. 2015;21(7):751-9.
40. Cejalvo JM, Martínez de Dueñas E, Galván P, García-Recio S, Burgués Gasión O, Paré L, et al. Intrinsic Subtypes and Gene Expression Profiles in Primary and Metastatic Breast Cancer. Cancer research. 2017;77(9):2213-21.
41. Oh HJ, Shin Y, Chung S, Hwang DW, Lee DS. Convective exosome-tracing microfluidics for analysis of cell-non-autonomous neurogenesis. Biomaterials. 2017;112:82-94.
42. Tyanova S, Temu T, Sinitcyn P, Carlson A, Hein MY, Geiger T, et al. The Perseus computational platform for comprehensive analysis of (prote)omics data. Nature methods. 2016;13(9):731-40.
43. Kramer A, Green J, Pollard J, Jr., Tugendreich S. Causal analysis approaches in Ingenuity Pathway Analysis. Bioinformatics (Oxford, England). 2014;30(4):523-30.
44. Szklarczyk D, Franceschini A, Wyder S, Forslund K, Heller D, Huerta-Cepas J, et al. STRING v10: protein-protein interaction networks, integrated over the tree of life. Nucleic acids research. 2015;43(Database issue):D447-52.

45. Pathan M, Keerthikumar S, Ang CS, Gangoda L, Quek CY, Williamson NA, et al. FunRich: An open access standalone functional enrichment and interaction network analysis tool. Proteomics. 2015;15(15):2597-601.
46. Pathan M, Keerthikumar S, Chisanga D, Alessandro R, Ang CS, Askenase P, et al. A novel community driven software for functional enrichment analysis of extracellular vesicles data. Journal of extracellular vesicles. 2017;6(1):1321455.
47. Shannon P, Markiel A, Ozier O, Baliga NS, Wang JT, Ramage D, et al. Cytoscape: a software environment for integrated models of biomolecular interaction networks. Genome research. 2003;13(11):2498-504.
48. Datta A, Kim H, Lal M, McGee L, Johnson A, Moustafa AA, et al. Manumycin A suppresses exosome biogenesis and secretion via targeted inhibition of Ras/Raf/ERK1/2 signaling and hnRNP H1 in castration-resistant prostate cancer cells. Cancer letters. 2017;408:73-81.
49. Hitosugi T, Kang S, Vander Heiden MG, Chung TW, Elf S, Lythgoe K, et al. Tyrosine phosphorylation inhibits PKM2 to promote the Warburg effect and tumor growth. Science signaling. 2009;2(97):ra73.
50. Yang W, Zheng Y, Xia Y, Ji H, Chen X, Guo F, et al. ERK1/2-dependent phosphorylation and nuclear translocation of PKM2 promotes the Warburg effect. Nature cell biology. 2012;14(12):1295-304.
51. Prakasam G, Iqbal MA, Bamezai RNK, Mazurek S. Posttranslational Modifications of Pyruvate Kinase M2: Tweaks that Benefit Cancer. Frontiers in oncology. 2018;8:22.
52. Zhao H, Yang L, Baddour J, Achreja A, Bernard V, Moss T, et al. Tumor microenvironment derived exosomes pleiotropically modulate cancer cell metabolism. eLife. 2016;5:e10250.
53. Al-Nedawi K, Meehan B, Micallef J, Lhotak V, May L, Guha A, et al. Intercellular transfer of the oncogenic receptor EGFRvIII by microvesicles derived from tumour cells. Nature cell biology. 2008;10(5):619-24.
54. Herst PM, Dawson RH, Berridge MV. Intercellular Communication in Tumor Biology: A Role for Mitochondrial Transfer. Frontiers in oncology. 2018;8:344.
55. Lou E, Zhai E, Sarkari A, Desir S, Wong P, Iizuka Y, et al. Cellular and Molecular Networking Within the Ecosystem of Cancer Cell Communication via

Tunneling Nanotubes. Frontiers in cell and developmental biology. 2018;6:95.
56. Warburg O, Wind F, Negelein E. THE METABOLISM OF TUMORS IN THE BODY. The Journal of general physiology. 1927;8(6):519-30.
57. Altenberg B, Greulich KO. Genes of glycolysis are ubiquitously overexpressed in 24 cancer classes. Genomics. 2004;84(6):1014-20.
58. Majumder PK, Febbo PG, Bikoff R, Berger R, Xue Q, McMahon LM, et al. mTOR inhibition reverses Akt-dependent prostate intraepithelial neoplasia through regulation of apoptotic and HIF-1-dependent pathways. Nature medicine. 2004;10(6):594-601.
59. Wiese EK, Hitosugi T. Tyrosine Kinase Signaling in Cancer Metabolism: PKM2 Paradox in the Warburg Effect. Frontiers in cell and developmental biology. 2018;6:79.
60. Gruning NM, Rinnerthaler M, Bluemlein K, Mulleder M, Wamelink MM, Lehrach H, et al. Pyruvate kinase triggers a metabolic feedback loop that controls redox metabolism in respiring cells. Cell metabolism. 2011;14(3):415-27.
61. Lee KM, Nam K, Oh S, Lim J, Lee T, Shin I. ECM1 promotes the Warburg effect through EGF-mediated activation of PKM2. Cellular signalling. 2015;27(2):228-35.
62. Yang W, Lu Z. Nuclear PKM2 regulates the Warburg effect. Cell cycle (Georgetown, Tex). 2013;12(19):3154-8.
63. Boisvert FM, van Koningsbruggen S, Navascues J, Lamond AI. The multifunctional nucleolus. Nature reviews Molecular cell biology. 2007;8(7):574-85.
64. Hamabe A, Konno M, Tanuma N, Shima H, Tsunekuni K, Kawamoto K, et al. Role of pyruvate kinase M2 in transcriptional regulation leading to epithelial-mesenchymal transition. Proceedings of the National Academy of Sciences of the United States of America. 2014;111(43):15526-31.
65. Amin S, Yang P, Li Z. Pyruvate kinase M2: A multifarious enzyme in non-canonical localization to promote cancer progression. Biochimica et biophysica acta Reviews on cancer. 2019;1871(2):331-41.
66. Zhou Z, Li M, Zhang L, Zhao H, Şahin Ö, Chen J, et al. Oncogenic Kinase-Induced PKM2 Tyrosine 105 Phosphorylation Converts Nononcogenic PKM2 to a Tumor Promoter and Induces Cancer Stem-like Cells. Cancer research. 2018;78(9):2248-61.

국 문 초 록

세포외 소포체에 의해 유도된 PKM2 인산화를 통한 관내강형 유방암 세포의 공격적 형질 획득

강서영

서울대학교

융합과학기술대학원

분자의학 및 바이오제약학과

호기성 당분 해는 암 포도당 대사의 특징이다. 여러 연구에서 암 유래 세포외 소포체(EV)는 인접 세포에서 포도당 대사를 조절하고 질병 진행을 촉진 할 수 있음을 보고하고 있다. 본 연구에서 우리는 호기성 당분해가 활성화되어 있는 암 세포에서 유래된 세포외 소포체가 상대적으로 당분해가 덜 활성화 되어있는 암 세포에서 포도당 대사를 조절하고 세포 증식을 유도할 수 있음을 제안한다.

암세포에서 유래된 세포외 소포체(EV)가 다른 종류의 암세포에

서 포도당 대사에 기여한다는 것을 입증하기 위해, 상이한 수준의 해당 활성을 갖는 2 가지 유형의 유방암 세포주(MDA-MB-231 및 MCF7)가 선택되었다. 트랜스-웰 세포배양 시스템 또는 미세유체 시스템과 같은 간접 공배양 시스템을 사용하여 두 세포를 공배양하여 수여자 세포(MCF7)에서 포도당 대사의 변화를 확인하였다. 플루오로데옥시글루코스(^{18}F-FDG)를 사용하여 이들 세포의 기본 포도당 대사 상태를 평가 하였다. 공초점 현미경을 사용하여 형광 단백질이 있는 공여 세포(MDA-MB-231-tdTomato)와 공동 배양된 수용 세포(MCF7)에서 세포외 소포체의 신호를 평가하였다. 해당 경로에서 중요한 단백질인 포도당 수송체(GLUT1)와 피루브산 키나아제 M2(PKM2)의 변화를 확인하기 위해서 웨스턴 블롯을 수행하였다. 수용 세포에서 전체 단백질들의 변화를 확인하기 위하여 단백질체 분석을 시행하였다.

60분간 FDG를 처리한 후, MDA-MB-231 및 MCF7 세포의 기본 FDG 흡수율은 매우 큰 차이를 나타냈다. 트랜스-웰 시스템을 이용하여 공여 세포(MDA-MB-231)과의 간접적 공동 배양 이후에 수용 세포(MCF7)의 FDG 흡수율이 크게 증가했다. 공여에서 분리된 세포외 소포체를 처리하고 24시간 배양 하였을 때, 수용 세포에서 FDG 흡수율이 증가하였으며 세포 증식 또한 증가하였다. 형광 단백질이 있는 공여 세포(MDA-MB-231-tdTomato)와 공동 배양한 후, 수용 세포(MCF7)의 공초점 현미경 촬영에서 세포 내부에 여러 개의 tdTomato 신호가 나타

났다. 이는 세포외 소포체(EV)가 공여 세포(MDA-MB-231-tdTomato)에서 비롯되어 수용 세포(MCF7) 내부로 이동했음을 입증했다. 웨스턴 블롯 분석 결과, 공여 세포와 공동 배양된 수용 세포에서 단일 배양된 수용 세포에 비해 포도당 수송체의 발현이 증가한 것으로 나타났다. 피루브산 키나아제 M2 (PKM2)의 발현 자체는 공동 배양된 수용 세포에서 큰 변화를 보이지 않았지만, 호기성 해당과정의 활성화를 암시하는 피루브산 키나아제 M2 (PKM2)의 인산화는 유의하게 증가하였다. 공동 배양된 수용 세포(MCF7)의 단백질체 분석에서 세포 증식 및 유전자 번역에 관련된 단백질들의 발현은 증가하였으나, 세포 분화와 관련된 단백질의 발현은 감소하였다. 또한, 세포외 소포체(EV)의 단백질체 분석은 세포외 소포체(EV) 내에 PKM2의 인산화를 위한 EGFR, ERBB2 및 MAPK와 같은 중요한 단백질이 있음을 밝혀냈다.

요약하면, 공여 세포(MDA-MB-231)에서 유래된 세포외 소포체(EV)는 피루브산 키나아제 M2 (PKM2)를 인산화함으로써 수용 세포(MCF7)에서 호기성 당분해를 활성화하였으며 이는 결국 수용 세포(MCF7)에서 세포 증식을 유도하였다. 이와 함께 공동 배양된 세포에서 세포증식과 관련된 단백질 발현은 증가한 반면, 세포 분화와 관련된 단백질들의 발현은 감소하였다. 따라서 이 현상은 공격적인 암 세포가 EV 매개자를 통해 다른 암 세포에 영향을 줄 가능성을 시사한다.

주요어: 유방암 세포, 세포외 소포체, 호기성 해당과정, 피루브산 인산화
학번: 2014-30803